molecular pharmaceutics

pubs.acs.org/molecularpharmaceutics

Article

Chiral and Dual Drugs Combination Reduces Tumor-Associated Neutrophils-Induced T-Cell Immunoparalysis to Treat Epithelial Ovarian Cancer

Yi Lai,[‖] Dan Ru,[‖] Hailang Dai,*[,‖] Chenhuan Ding, Ling Ding, Chen Wang, Cenxin Luo, Yujie Qi, Xianfeng Chen,* and He Li*

Cite This: *Mol. Pharmaceutics* 2026, 23, 694−710

Read Online

ACCESS | Metrics & More | Article Recommendations | Supporting Information

ABSTRACT: In antitumor activities, baicalin and astragaloside IV inhibit tumor growth, induce cell death, and restrain metastasis in various cancers. Generally, a mixture of massive herbs like scutellaria or astragalus matches with other drugs to reach a curative effect in traditional Chinese prescription. Therefore, researchers aspire to an effective type of drug combination that shows promoted absorption and higher bioavailability in preclinical studies. Here, we report an optical method to detect chiral baicalin and astragaloside IV and also monitor the absorption of different chirals in ovarian cells. Eventually, R-Baicalin-Astragaloside IV dual drugs combination shows promoted absorption of each other compared with single chiral drugs or another. Based on the optical method results, we designed a series of in vitro and in vivo experiments to explain and analyze the mechanism of the curative effect. Therein, the result reveals that the tumor-associated neutrophils were reduced via the down-regulated TLR4/MYD88/NF-κB pathway to increased PD-1/PD-L1 immune response in epithelial ovarian cancer under the influence of R-Baicalin-Astragaloside IV. Thus, this work offers a comprehensive report on structure−activity relationships of chiral and dual drug strategies to improve its bioavailability in therapy of ovarian cancer.

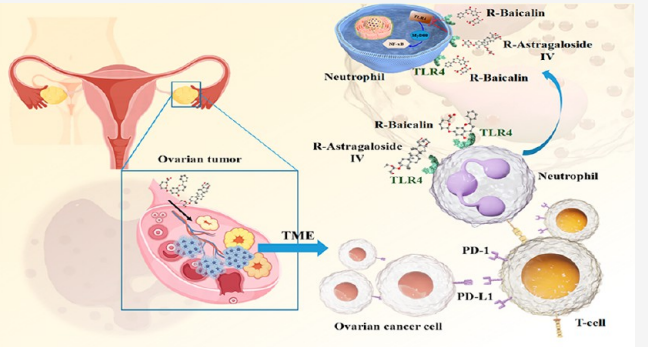

KEYWORDS: *chiral dual drugs, photonic waveguide sensor, baicalin−astragaloside IV, ovarian cancer, neutrophils*

1. INTRODUCTION

Ovarian cancer (OC) is one of the most deadly gynecological tumors, of which epithelial OC (EOC) is the most common pathological type, accounting for 50−70%.[1] Nearly three-quarters of patients are diagnosed at stage III or IV, and most of them die within 18 months due to primary treatment resistance or recurrence.[1,2] Despite extensive biological research and clinical trials conducted over the years, the overall survival (OS) of patients has not improved significantly, so effective new therapies are urgently needed. Therein, immune checkpoint blocking (ICB) induces effective immunobinding therapies, such as programmed cell death (PD-1) or its ligand (PD-L1) antibodies, but these effects are observed in only 20−30% of patients, and even lower in OC, as low as 5.9−21%, with a median response rate less than 15%.[3] A variety of immune cell types exist in the tumor microenvironment (TME), including macrophages, dendritic cells, neutrophils, natural killer cells, B cells, and T cells.[4] Recent studies have shown that these immune cells play an important anticancer or cancer-promoting role. The functional and phenotypic status of immune subsets plays an important role in determining response to ICBs, among which the therapeutic effect is related to effective T cell status and intact host PD-L1 and PD-1 signaling pathways.[5,6] Most OC tumors have low levels of T cell infiltration and exhibit a "desert" T cell phenotype,[6] so that OC immunotherapy has long been neglected. Actually, T cell cloning and proliferation can be regulated by other immune cells in TME, such as tumor-associated neutrophils (TANs) which promote cancer cell proliferation, metastasis, and angiogenesis via promoting T cell IFN-γ production and inhibiting antitumor T cell response.[7] Neutrophils are the most abundant immune cells and infiltrate every part of the human body; multiple studies have found that the importance of neutrophils in cancer is becoming increasingly apparent; thus, the idea that neutrophils are just a bystander in TME is no longer there. In pancreatic cancer, higher TANs density predicted poorer OS, while higher infiltration of CD8 + GZMB + T cells was associated with improved survival.[8,9]

Received: May 9, 2025
Revised: November 28, 2025
Accepted: December 4, 2025
Published: January 8, 2026

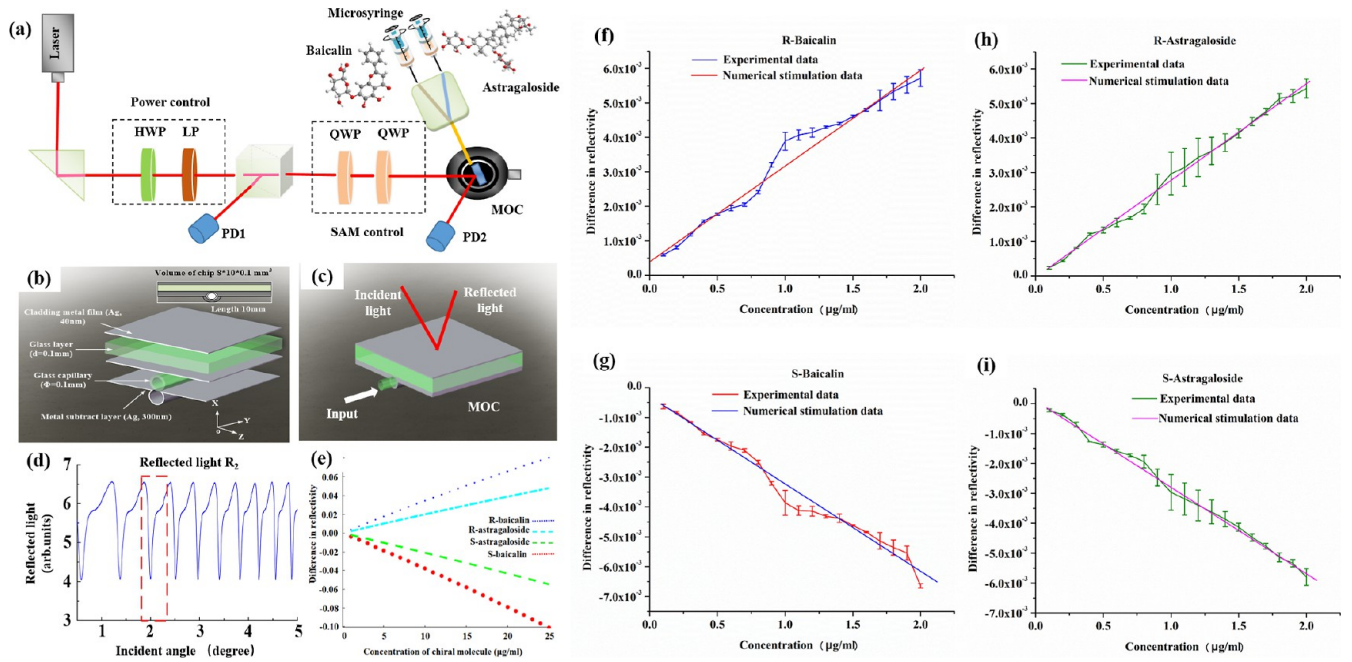

Figure 1. Schematic of the MOC and the discerning process and experimental setup and the results of the prepared chiral molecule solution experience. (a) Schematic of the experimental setup, which consists of a combination of a HWP and linear polarizer, QWPs, PDs, MOC, and a microsyringe system. (b) Schematic diagram of the MOC. The thickness of the coupling layer ranges from 30 to 50 nm, and the metal substrate is about 300 nm. The guiding layer which contains an outside capillary with a radium of 0.1 mm and a 1.1 mm thick glass slab. (c) The excitation of UOMs via a free space coupling technique in MOC (reflective is R1). (d) A series of the reflectivity R1 spectrum of the modes with respect to the incident angle and a mode at a coupling angle at the MOC, respectively. (e) Theoretical results of the difference in reflectivity when kinds of sample injected into cavity. (f–i) The experimental results of R/S-baicalin and the R/S-AS-IV solution with different concentrations, respectively.

Therefore, the regulation of neutrophils to modulate T cells and enhance the immune response to ICB is emerging as a novel tumor therapeutic approach.

Baicalin, as a flavonoid isolated from the *Scutellaria baicalensis* plant, astragaloside IV (AS-IV), as a saponin compound isolated from astragaloside, have various pharmacological activities, including antitumor, antimicrobial, and antioxidant, and has wide clinical applications.[10−14] Meanwhile, they can play a role in antitumor activities by regulating the TME and tumor cell growth cycle.[15−17] Therefore, we hope to explore the potential targets and mechanisms of baicalin and AS-IV in the immunotherapy of OC, so as to find a new method of TCM assisted tumor immunotherapy. In this work, we report a metal-cladding optofluidic cavity (MOC) method to detect chiral baicalin and AS-IV, and also monitor the absorption of different chirals of baicalin and AS-IV in ovarian cells. As a result, R-Baicalin and R-AS-IV combination show promoted absorption of each other compared with single chiral drugs. In contrast, S-baicalin and S-AS-IV present inhibition of each. Based on the detection, we designed a series of in vitro and in vivo experiments to analyze this phenomenon. Therein, the result reveals that the TANs were reduced via down-regulated TLR4/MYD88/NF-κB pathway to increase PD-1/PD-L1 immune response in EOC under the influence of R-baicalin-AS-IV. Thus, this paper offers a comprehensive report on pharmacokinetic behavior of chiral and dual drug strategies to improve its bioavailability and immunocompetence in the therapy of OC.

2. MATERIALS AND METHODS

2.1. Metal Cladding Optofuidic Chip

The MOC possesses a variety of fascinating optical properties.[53,54] The most unique feature is the excitation of ultrahigh-order guided modes (UOMs) in the cavity under illumination. Moreover, the reflective coefficient of UOMs is extremely sensitive to the dielectric coefficient of the guided layer. For the MCOC, the reduced dispersion equation for the *m*-order eigenmode can be written as

$$k_0 d\sqrt{n^2 - N_{\text{eff}}{}^2} = m\pi \tag{1}$$

where N_{eff} is the effective refractive index. The incident beam meeting coupling conditions (the component of wave vector along propagation direction resonates with the propagation constant of the eigenmodes) will be coupled into the waveguide, resulting in coupling peaks. The coupling peak is particularly sensitive to the refractive index that the sensitivity s is defined as

$$s = \frac{\mathrm{d}N_{\text{eff}}}{\mathrm{d}n} = \frac{n}{N_{\text{eff}}} \tag{2}$$

where the sensitivity approaches infinity with N_{eff} approaching zero in UOMs.[55]

Based on the properties, we demonstrated the discrimination of two pairs of chiral molecules in cell and animal experiments. As shown in Figure 1a, the intensity of LCP/RCP shows a difference in reflective light when the chiral molecule is injected into MCOC due to the different dielectric coefficients of the chiral molecules for LCP and RCP. The difference in reflectivity of LCP/RCP, D can be expressed as (see more details in Supporting Information Section SI)

$$D = K\Delta\varepsilon_2 \tag{3}$$

where $\Delta\varepsilon_2$ is the change in the dielectric coefficient for LCP light (thus, $-\Delta\varepsilon_2$ for RCP light). *K* is the characteristic parameter determined by the MCOC. Therefore, the difference in reflectivity of LCP and RCP will be characterized by opposite signs for a pair.

2.2. Cell Culture

The OC cell lines SKOV3 and ID8 were purchased from the National collection of authenticated cell cultures (Shanghai, China). All cell lines were cultured in Dulbecco's modified Eagle's medium (DMEM)

https://doi.org/10.1021/acs.molpharmaceut.5c00681
Mol. Pharmaceutics 2026, 23, 694−710

supplemented with 10% fetal bovine serum (FBS) and penicillin−streptomycin antibiotic mixture (Gibco) at 37 °C in an atmosphere of 5% CO_2.

2.2.1. CCK8 Assay. Cell viability was detected via a cell counting kit-8 (CCK-8) assay. SKOV3 cell lines were incubated with baicalin, AS-IV or dual drugs for 24−48 h, and then replaced with 100 μL 10% CCK-8 reagent (TargetMOI, China) for 1 h at 37°C. The OD of each well was measured at 450 nm using a Thermo Scientific Varioskan Flash (Thermo Fisher Scientific, USA).

2.2.2. EdU Staining. The cell proliferation was measured using the EdU assay kit according to the manufacturer's instructions. Briefly, the cells in the 6-well plates were exposed to different drugs for 24 h at 37 °C in an atmosphere of 5% CO_2, 10 μmol/mL EdU for 2 h, fixed with 4% formaldehyde for 15 min, and permeabilized in 0.3% Triton X-100 for 10 min. Then, the cells were incubated with click additive solution for 20 min. The cells were labeled using 200 μL streptavidin-HRP for 30 min and DAB solutions for 30 min. The cells were imaged by a microscope (Olympus America Inc., USA), and the number of EdU positive cells was counted from 3 random fields in each well.

2.2.3. Cell Invasion and Migration. Cell invasion and migration was measured using a 24-well Transwell chamber (Corning Costar) precoated with or without Matrigel. Cells in the serum-free medium with different drugs were seeded at 1×10^5 per well in the top chamber, while 20% FBS in the DMEM medium was added in the bottom chamber. After incubation for 24 h at 37 °C, the cells were fixed with 4% formaldehyde for 15 min, stained with 0.5% crystal violet for 15 min, and counted.

2.2.4. Wound Healing. SKOV3 cells were seeded at a concentration of 1×10^5 cells/well into 12-well plates in DMEM supplement. Cells were incubated overnight, yielding a confluent monolayer for wounding. Wound tracks in the monolayer were scored in each well using a 200 μL pipet tip. Then, the suspended cells were washed twice with PBS, and the wounded cell monolayer was incubated in 5% FBS medium with different drugs for 24 h. Photographs of the wound area were captured at 0 and 24 h with a microscope (Olympus America Inc., USA).

2.2.5. qPCR. Total RNA was extracted from cells and then reverse-transcribed into cDNA using EZ-press RNA purification (EZ bioscience). qPCR was performed on the Bioer/LineGene 9600 detection system with an SYBR Premix ExTaq Kit (Takara). The data were normalized to the expression of GAPDH. The sequences of the primers are given in Table S3.

2.3. Animals and the In Vivo Model

All animal experiments were performed in accordance with the National Guidelines for Animal Care and were approved by the Animal Experiment Ethics Committee of Shanghai Renji hospital affiliated to Shanghai Jiao Tong University School of Medicine (approval number: R52022−0921, approval date: 2022.09.14).

2.3.1. Animal Treatments. Mice were maintained under specific pathogen free conditions to ensure compliance with the 3R principles and were randomly assigned to each experimental group. All mice were supplied with sterile drinking water and were fed freely. Six to eight week old female BALB/c-nu and C57BL/6 mice were used for the studies. BALB/c-nu mice were injected with 5×10^6 SKOV3 cells, while C57BL/6 mice were injected with 5×10^6 ID8 cells. All cells were injected subcutaneously into the flank. Details of the specific animal experimental procedures are provided in the Supporting Information (Section S3).

2.4. RNA Sequencing

Total RNA from tumor tissues was extracted with Trizol Reagent (Invitrogen Life Technologies, Carlsbad, CA, USA) and assessed with an Agilent 2100 Bioanalyzer (Agilent Technologies, Santa Clara, CA, USA) and a NanoDrop spectrophotometer (Thermo Scientific, Waltham, MA, USA). Total RNA samples that met the following requirements were used in subsequent experiments: an RNA integrity number (RIN) > 8.0 and A260/A280 = 1.8−2.0. Libraries were sequenced on the Illumina NovaSeq 6000 platform (Illumina, San Diego, CA, USA) at Shanghai Personal Biotechnology Co., Ltd. (Shanghai, China), generating 150 bp paired-end reads. Each sample was sequenced to a depth of ≥6 Gb clean data (approximately 20 million paired-end reads). We used HTSeq (0.9.1) statistics to compare the Read Count values on each gene as the original expression of the gene and then used FPKM to standardize the expression. Then, different expression of genes was analyzed by DESeq (1.39.0) with different expression of multiple |log2FoldChangel > 1, significant P-value <0.05. Differences in gene expression profiles between the two groups were represented by volcano maps, with vertical dashed lines representing up-regulated and down-regulated differences of 2.0 times (log2 conversion), and differentially expressed genes was drawn by the R language ggplots2 software package. In order to further analyze the function of differentially expressed genes after dual drugs administrations, we used top GO to conduct the related analysis of GO enrichment and KEGG pathway to annotate the differential genes and the gene list and the number of each pathway, and the hypergeometric distribution method was used to obtain P values ($P < 0.05$). Use genes cloud platform (https://www.genescloud.cn) for data analysis, and heatmap package (V1.0.8) developed by heat map tool drawing heat maps.

2.5. Extraction of Peripheral Blood Mononuclear Cells

Mice blood and spleen were collected after sacrifice, and lymphocyte separation solution (Dakewe Biotech, 7211011) was added into 15 mL centrifuge tube. Peripheral blood was diluted by RPMI 1640; spleen was ground and then filtered with 70 μm biofilters, then mixed fluid was spread on the upper surface of the solution; 800 g centrifuge for 20 min at room temperature. After centrifugation, the lymphocytes were then washed and counted.

2.6. Isolation of Single Cell Suspension

The subcutaneous tumor tissues of mice were separated and washed twice with PBS. The fat and peripheral tissue were removed, cut into small pieces, and then single cells were extracted using the mouse tumor dissociation kit (Miltenyi Biotec, 130-096-730). 100 μL Enzyme D, 10 μL Enzyme R, and 12.5 μL Enzyme A were added into 2.35 mL RPMI 1640 medium and inserted into gentleMACS C Tube together with tumor tissues. The gentleMACS program was started: m_impTumor_02, and vibrated at 37 °C for 45 min. The gentleMACS program was started: 1 × m_impTumor_03. The solution was filtered using a 70 μm filter and the filter was slowly rinsed using 15 mL RPMI 1640 medium; 300 g centrifuge for 7 min at room temperature. After centrifugation, the supernatant was removed to acquire a single cell suspension.

2.7. Extraction and Functional Assays of TAN

Neutrophils were extracted from the tumor by a neutrophil enrichment kit (stemcell, 19762). Details of the specific experimental procedures are provided in the Supporting Information (Section S10).

2.7.1. ROS Detection. ROS concentration of TANs was conducted by a reactive oxygen species assay kit (beyotime, S0033S). Cells were washed three times with PBS and then loaded with 20 μM DCFH-DA in fresh medium for 30 min. After three additional PBS washes, the cells were analyzed by flow cytometry.

2.7.2. IL-6 Detection. IL-6 concentration of TANs was performed by a Mouse IL-6 ELISA Kit (beyotime, PY2782). 50 μL of the standard diluent and samples were added to the plate, and the plate was sealed with a sealing film, and incubated at room temperature for 120 min. The wash was repeated by washing buffer, and the plate was pat dried after the last wash. Then, 100 μL of the TMB solution was added to each well. The plate was sealed and incubated at room temperature for 20 min. Then, 100 μL stop solution was added to each well to terminate the reaction. A microplate reader was used to measure the absorbance at 450 nm.

2.8. Flow Cytometry

The cell suspension was stained with Zombie Aqua (Biolegend 423101) to exclude dead cells. Then use APC antihuman/mouse Granzyme B Recombinant (clone QA16A02) Biolegend 372203; APC antimouse Ly6G (clone 1A8) Biolegend 127613; PerCP/Cyanine5.5 Antimouse CD45 (clone 30-F11) Biolegend 103131; FITC Anti-mouse/human CD11b (clone M1/70) Biolegend 101205; FITC

https://doi.org/10.1021/acs.molpharmaceut.5c00681
Mol. Pharmaceutics 2026, 23, 694−710

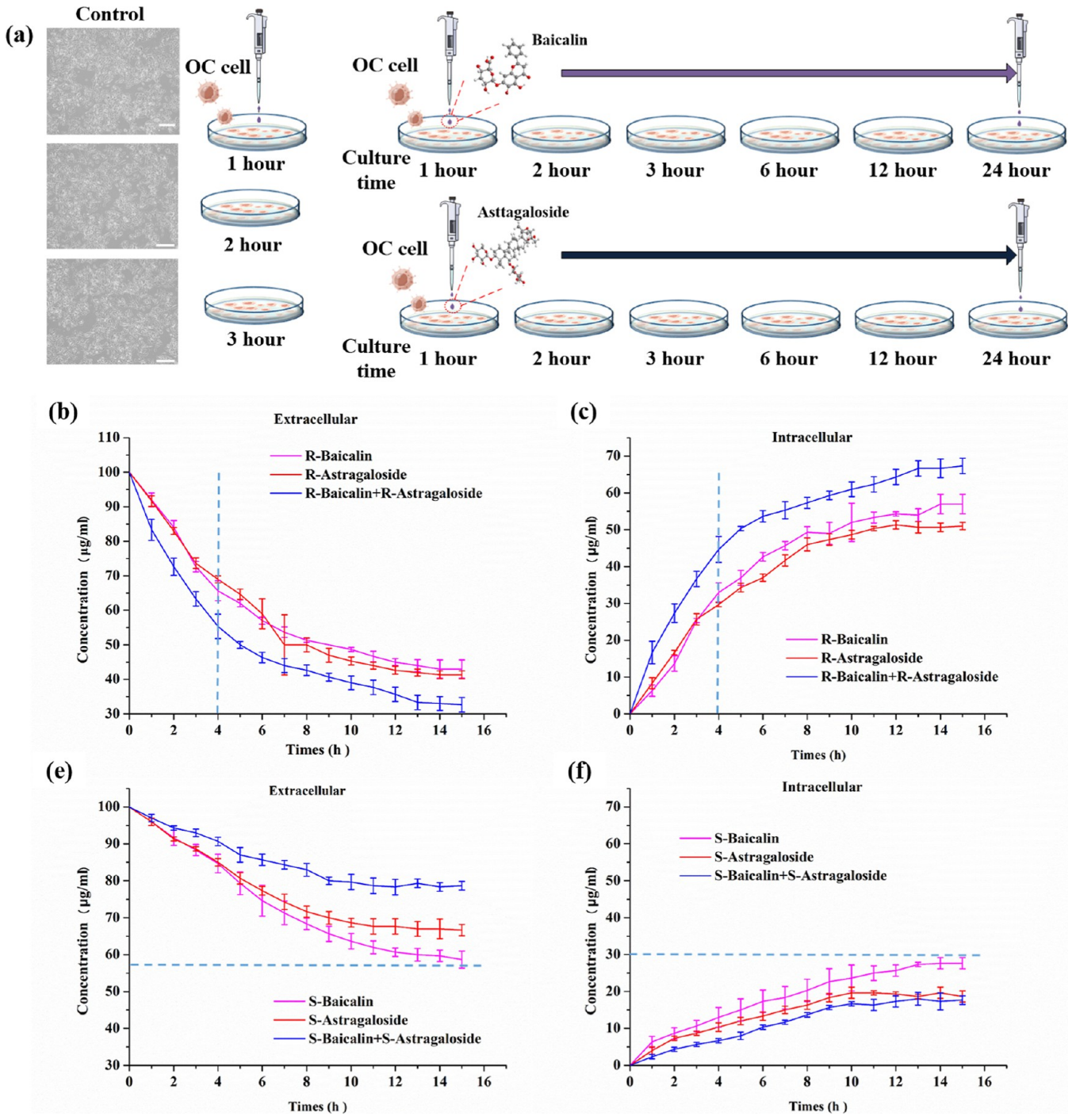

Figure 2. Effect of chiral baicalin, astragaloside (AS-IV), and the combination of two drugs on cell growth and cell viability, respectively. (a) OC cells were cultured with baicalin and AS-IV at a concentration of 100 μm. After 1 h, 2 h, 3 h, 6 h, 12 h, and 18 h of culture, the culture medium and intracellular fluid were sampled to detect changes in the concentration (see Methods). (b,c) Various concentrations of R-/S-baicalin and R-/S-AS-IV in the culture medium and intracellular with different culture times, respectively.

Antimouse CD8a (clone 53−6.7) BioLegend 100705, PE antimouse CD279 (PD-1) Antibody (clone 29F.1A12) BioLegend 135205 to dye cells for 15 min. After staining, the samples were washed twice with PBS and resuspended in the staining buffer. The samples were detected by an LSR Fortessa X-20 and Celesta Flow cytometry system and analyzed by Flow Jo software.

2.9. Western Blot

Cells were lysed in RIPA buffer containing protease inhibitors, and protein concentrations were determined by using a BCA assay. Samples were denatured by boiling in loading buffer (5 min, 100 °C), and then, equal amounts of protein (20−50 μg) were separated by sodium dodecyl sulfate−polyacrylamide gel electrophoresis (12% gel) at 110 V for 1.5 h. Next, proteins were transferred onto PVDF membranes using a wet transfer system (200 mA, 1.5 h, 4 °C) and blocked with blocking buffer for 1 h at room temperature. Primary antibodies such as β-actin (A01015,1:5000, Abbkine); TLR4 (19811−1-AP,1:1000, Proteintech), MYD88 (67969−1-Ig,1:1000, Proteintech); and NF-κB (80979−1-RR,1:1000, Proteintech) were diluted and incubated overnight at 4 °C. Membranes were washed 3 times with TBST, then incubated with HRP-conjugated secondary antibodies (1:5000) for 1 h

https://doi.org/10.1021/acs.molpharmaceut.5c00681
Mol. Pharmaceutics 2026, 23, 694−710

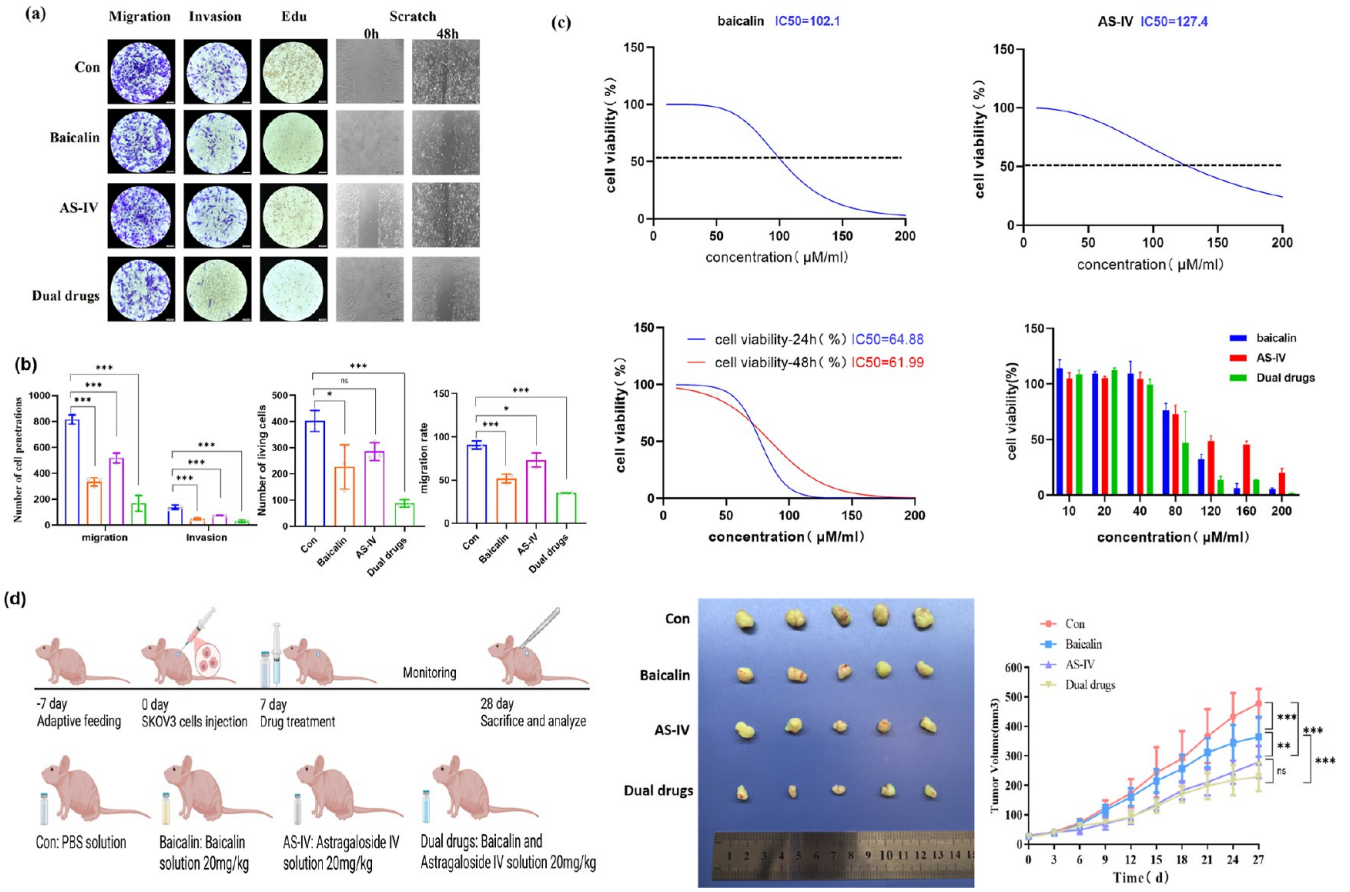

Figure 3. The proliferation, migration and invasion of SKOV3 cell lines under different drugs, and tumor growth of BALB/c-nu mice treated with single and dual drugs. (a) The transwell, EdU staining, and scratch assay of SKOV3 cell lines under different drugs. (b) Quantitative statistics of a. (c) 24 h cell viability and half-maximal inhibitory concentration (IC50 value) of SKOV3 cell line under single and dual drugs. (d) Transplanted tumor treated with single and dual drugs. The growth curve of transplanted tumor in BALB/c-nu mice treated with single and dual drugs. $^{*}P < 0.05$, $^{**}P < 0.01$, $^{***}P < 0.001$, ns had no statistical difference.

at RT. β-actin served as a loading control. Results were visualized using the ECL substrate and quantified by ImageJ software.

2.10. Immunofluorescence

The mice tissues were fixed with formaldehyde and embedded in paraffin. Subsequently, the tissue samples were cut into 4 μm thicknesses, deparaffinized in xylene, and rehydrated through graded ethanol solutions to analyze PD-1, CD8 expression, and neutrophil infiltration. The sections were deparaffinized and rehydrated and then blocked with 3% bovine serum albumin for 30 min. The sections were next incubated with anti-Ly6G antibody (1:300, #88876s, CST); CD8, PD-1(Proteintech, China) overnight at 4 °C and Cy3-labeled secondary antibody for 1 h at 37 °C, followed by nuclear staining with DAPI for 10 min at room temperature. Co-localization of MYD88 and Ly6g was performed by anti-Ly6G antibody (1:300, #88876s, CST) and Alexa Fluor 555-labeled secondary antibody, MYD88(1:200, #23230-1-AP, Proteintech) and Alexa Fluor 488-labeled secondary antibody, respectively. The staining results were observed with images acquired using a Nikon confocal laser microscope (Eclipse Ti-SR, Nikon) and an imaging system (DS-U3, Nikon). The fluorescence intensity quantification were analyzed with the ImageJ software.

2.11. Immunohistochemistry and HE Staining

After routine deparaffinization, rehydration, and antigen retrieval, the sections were incubated with monoclonal antibodies against TLR4, MYD88, NFKB, PD-L1(Proteintech, China) at 4 °C overnight, followed by incubation with the corresponding secondary antibodies at 37 °C for half an hour and visualization using DAB. The average optical density image was analyzed with the ImageJ software.

2.12. Binding Affinities and Modes of Interaction

To analyze the binding affinities and modes of interaction between the drug candidate and their targets, AutodockVina 1.2.2, a silico protein−ligand docking software was employed. The molecular structures of TLR4 and MYD88 was retrieved from PubChem Compound (https://pubchem.ncbi.nlm.nih.gov/). The three-dimensional coordinates of TLR4 (PDB ID, 4R7D; resolution, 2.753 Å) and MYD88 (PDB ID, 4DOM; resolution, 1.798 Å) were downloaded from the PDB (http://www.rcsb.org/pdb/home/home.do). For docking analysis, all protein and molecular files were converted into PDBQT format with all water molecules excluded, and polar hydrogen atoms were added. The grid box was centered to cover the domain of each protein and accommodate free molecular movement. The grid box was set to 30 Å × 30 Å × 30 Å, and the grid point distance was 0.05 nm. Molecular docking studies were performed by Autodock Vina 1.2.2 (http://autodock.scripps.edu/).

2.13. XPS Analysis

The Thermo Scientific Nexsa G2 was used for the test: monochromatized Al target (1486.6 eV), a test beam spot size of 400 μm, a full spectrum pass energy of 100 eV, a step size of 1.0 eV, a narrow spectrum pass energy of 50 eV, a step size of 0.05 eV, and the X-ray was at a 30° angle to the horizontal plane. The neutralizer gun was kept on throughout the process to alleviate uneven charging.

2.14. Statistical Analysis

Statistical analyses were conducted using Graphpad Prism 8 software. Results are expressed as mean ± standard error of the mean. The significance of differences among experimental groups was determined

https://doi.org/10.1021/acs.molpharmaceut.5c00681
Mol. Pharmaceutics 2026, 23, 694−710

by ANOVA analysis. The differences are considered statistically significant at $p < 0.05$.

3. RESULTS

3.1. Chiral and Dual Drugs Promoted the Therapeutic Effective by MOC Detection

To demonstrate the ability to distinguish chiral molecules, we measured the difference in the reflectivity of prepared baicalin and AS-IV solutions. The results showed that the difference in reflectivity of two pairs of chiral molecules is proportional to the concentration with the opposite sign coefficient, which is consistent with theoretical predictions (Figure 1b,c and Supporting Information Section S1). The experimental setup is shown in Figure 1a. The power and spin angular momentum of the laser beam (generated by a 100 mW 632.8 nm laser beam) are controlled by a combination of a half-wave plate (HWP), a quarter-wave plate, and a linear polarizer (LP). Two photoelectric detectors (PDs) are used to detect the incident and reflective beam intensities. The samples of the prepared chiral molecule solution are injected into the MOC with a microsyringe system (the part I of Supporting Information). Then, the reflectivity of LCP/RCP is detected to generate a difference in reflectivity. After each experiment, a blank buffer was used to wash the cavity. Figure 1f−i shows the experimental results of the prepared chiral molecule solution, in which the difference in reflectivity is positive and negative for R-structure molecules (R-baicalin and R-AS-IV) and S-structure molecules (S-baicalin and S-AS-IV), respectively. Its absolute value increased linearly with the concentration of chiral molecules, with correlation coefficients of $0.00290 \pm 0.00006/-0.00292 \pm 0.00005$ mL·mg^{-1} for R-/S-baicalin and $0.00279 \pm 0.00007/-0.00301 \pm 0.00005$ mL·mg^{-1} for R-/S-AS-IV. Therefore, the experimental results of the prepared chiral molecule solution are consistent with the theoretical results. Moreover, the changing intensity of the light induced by the optical rotation for the ADP is 0.00084 mL·mg^{-1}, indicating that the sensitivity of MOC is greater than the optical rotation.

In the following section, we will use the experimental results shown in Figure 1h−i as the calibration data to detect the concentrations of R-/S-baicalin and R-/S-AS-IV at intracellular and extracellular levels of OC cell, respectively, as shown in Figure 2a. First, OC cells were coincubated with the same concentrations of chiral drugs (R-/S-baicalin or R-/S-AS-IV) from 0 to 18 h. As shown in Figure 2b−f and (the part I of Supporting Information), compared with the concentration of R-/S-baicalin or R-/S-AS-IV at the extracellular (culture solution) and intracellular levels, the R-baicalin and R-AS-IV had a good absorption on the OC cell, respectively. Moreover, the effects of absorption reinforce each other when R-baicalin and R-AS-IV were added into the culture medium at the same time by 1:1 concentration. In contrast, the amount of S-baicalin and S-AS-IV, S-baicalin and R-AS-IV, and R-baicalin and S-AS-IV absorption obviously decreased compared to R-baicalin and R-AS-IV, as shown in Figures 2b−f, S3 and S4. Meanwhile, the combination of S-baicalin and S-AS-IV had reciprocal inhibitory absorption when added into culture. These phenomena are consistent with our results, confirming that baicalin and AS-IV own an inhibitory effect on OC cells and vary between different chiral drugs. In conclusion, the combination of R-baicalin and R-AS-IV promoted the therapeutic effective in OC.

3.2. Dual Drugs Exhibit Better Therapeutic Efficacy than Single Drugs in OC

As shown in Figure 3a−c, it was found that both drugs could inhibit the proliferation, migration, and invasion of the SKOV3 cell line, and the inhibitory effect was enhanced with the increase of concentration. The 24 h IC50 values of baicalin and AS-IV for SKOV3 cell line were 102.1 and 127.4 μm, respectively. At the same time, dual drug significantly reduced cell proliferation compared with single drug ($P < 0.05$), and the IC50 at 24 and 48 h was 64.88 and 61.99 μm respectively, in Figure 3c.

The coefficient of drug interaction (CDI) was used to evaluate the synergistic effect between baicalin and AS-IV, and the synergistic effect was quantized according to the formula $CDI = AB/(A \times B)$, where AB is the survival fraction of dual drugs treatment, and A and B are the survival fraction of single treatment. CDI < 1 indicates synergy, CDI = 1 indicates additivity, and CDI > 1 indicates antagonism. As shown in Table 1, baicalin and AS-IV have synergistic effects at all concentrations, and the synergistic effects are strongest at 60 and 90 μm concentrations. According to synergy scores in Section S2 of Supporting Information, the most synergistic area was baicalin ranging 60−120 μM with AS-IV ranging 60−120 μM at 24 h, and baicalin ranging 30−90 μm with AS-IV ranging 30−90 μm at 48 h (Figure S6). Therefore, we concluded baicalin and AS-IV had a strong synergistic effect, and the recommended concentration was 60 μm baicalin with 60 μm AS-IV in OC.

Table 1. CDI of Dual Drugs

	AS-IV (μM)				
	CDI (24 h/48 h)				
bai (μM)	10	30	60	90	120
10	0.96/0.98	0.95/0.91	0.77/0.76	0.75/0.59	0.63/0.71
30	0.99/0.91	0.88/0.88	0.74/0.65	0.78/0.52	0.59/0.62
60	0.97/0.85	0.92/0.85	0.67/0.43	0.63/0.41	0.48/0.53
90	0.99/0.98	0.97/0.88	0.67/0.44	0.66/0.25	0.13/0.19
120	0.94/0.90	0.92/0.91	0.51/0.50	0.56/0.28	0.05/0.14

In addition, the SKOV3 cell suspension was injected subcutaneously in BALB/c-nude mice and randomly divided into four groups, as shown in Figures 3d and S7. All animal experiments were performed in accordance with the national and institutional guidelines for animal care and approved by the Animal Experiment Ethics Committee of Shanghai Renji hospital affiliated to Shanghai Jiaotong University School of Medicine (approval number: R52022-0921, approval date: 2022.09.14). The mice were fed PBS, baicalin 20 mg/kg, AS-IV 20 mg/kg, and dual drugs 20 mg/kg once a day. It was found that the tumor of the baicalin group was significantly smaller than the control group, $P < 0.001$; the tumor of the AS-IV group was significantly smaller than that of the control and baicalin groups, $P < 0.01$; the tumor of the dual drugs group was significantly smaller than that of the control and baicalin groups, $P < 0.001$. It can be seen that the dual drugs can effectively inhibit the growth of OC tumors, especially in C57 mice (Figure S8). Collectively, these results reveal that the dual drugs could significantly inhibit the migration and invasion of the SKOV3 cell line and inhibit the growth of the OC tumor.

https://doi.org/10.1021/acs.molpharmaceut.5c00681
Mol. Pharmaceutics 2026, 23, 694−710

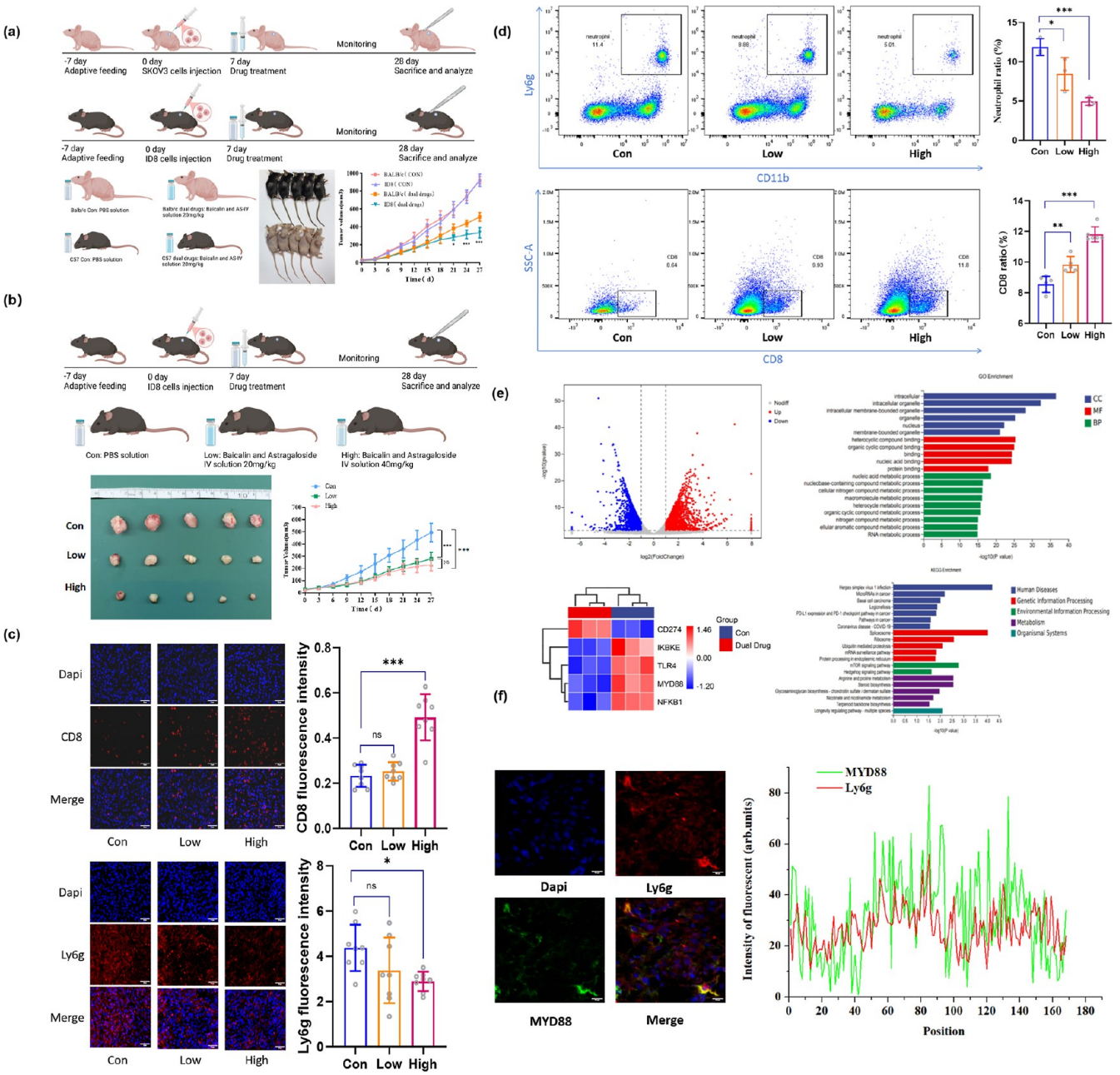

Figure 4. Tumor growth and expression of CD8 T cells and neutrophils of C57 mice treated with dual drugs at different concentrations, differential genes and functional analysis between dual drugs and control group, colocalization of MYD88 and Ly6g in EOC. (a) Transplanted tumor in C57 and BALB/c-nude mice under dual drug treatment. (b)Transplanted tumor and growth curve of C57 mice at different concentrations. (c) The immunofluorescence intensity of CD8 and Ly6g in tumor tissues under different drug concentrations (magnification × 400) and quantitative statistics, $*P < 0.05$, $**P < 0.01$, $***P < 0.001$, ns had no statistical difference. (d) Flow cytometry detected the proportion of neutrophils and CD8 + T cells of PBMCs under different drug concentrations and quantitative statistics. (e) Volcano map, GO and KEGG functional analysis of differential genes, heat map analysis of TLR4/MYD88/NF-κB genes in C57 mice between two groups. (f) The immunofluorescence intensity and gray values of green (MYD88) and red (Ly6g).

3.3. Dual Drugs Increase the CD8 + T Cell and Reduces TANs in OC

It was found that dual drug owned better inhibitory effects in C57 mice than BALB/c-nude mice (Figure S9), which indicated immune cell involvement. Therefore, ID8 cell suspension was injected subcutaneously in C57 mice and randomly divided into three groups to reveal changing of immune cells. The mice were fed PBS, dual drugs 20 mg/kg, and 40 mg/kg once a day. It was found that the tumor of the low and high group was significantly smaller than the control group, $P < 0.001$, as shown in Figures 4b and S10, which inferred that the dual drugs can effectively inhibit the growth of OC tumors. Next, peripheral blood mononuclear cells (PBMCs) in spleen and peripheral blood were isolated, respectively, according to manufacture protocols (Section S5). The proportion of CD8 + T lymphocytes and neutrophils in PBMCs were analyzed by flow cytometry, and the expression of their markers in tumor tissues was analyzed by immunofluorescence.

After 28 days of administration, the neutrophils ratio of three group was 11.87 ± 1.08, 8.46 ± 2.09, and 4.95 ± 0.48. The

https://doi.org/10.1021/acs.molpharmaceut.5c00681
Mol. Pharmaceutics 2026, 23, 694−710

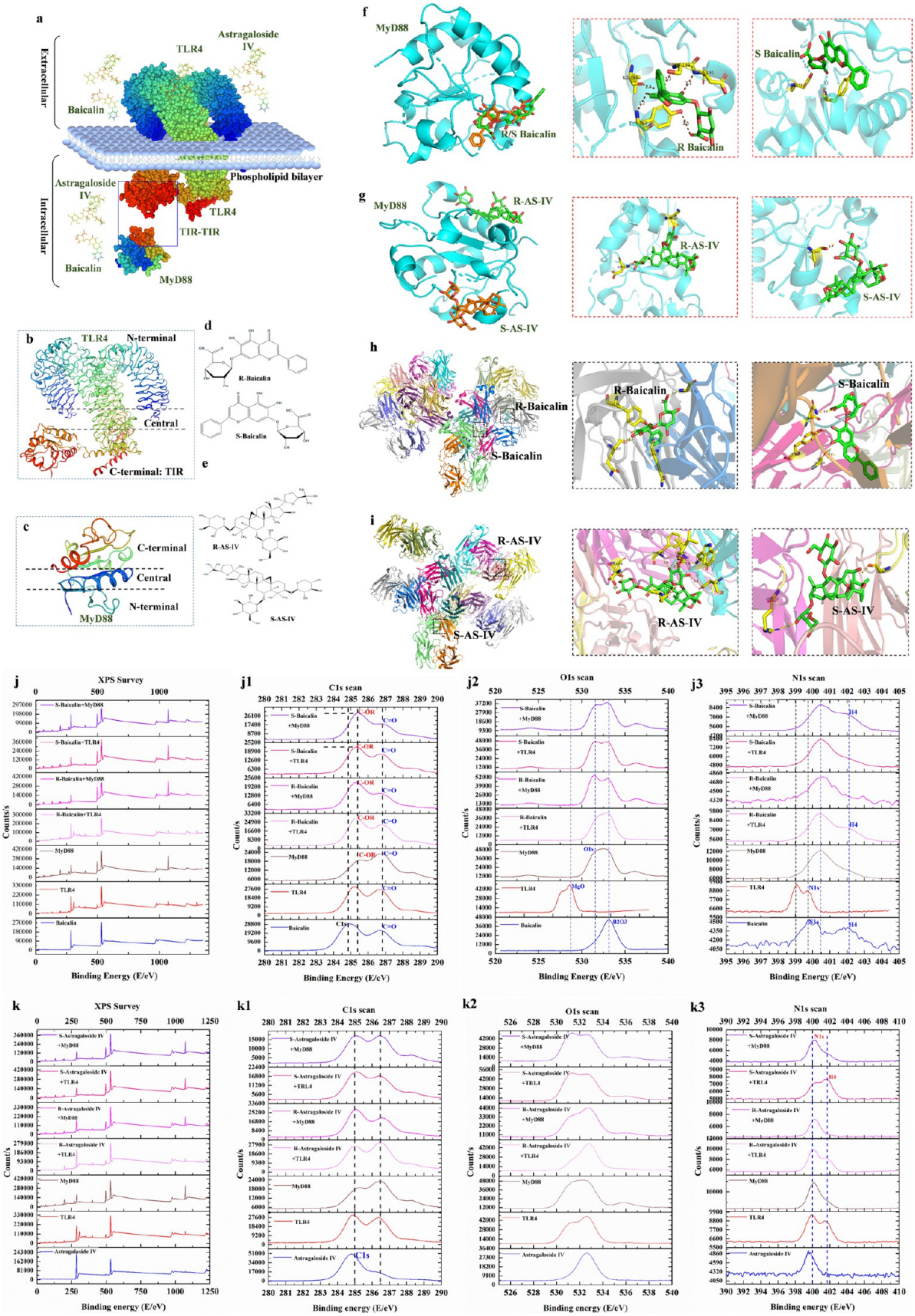

Figure 5. The molecular docking analysis. The molecular docking analysis. (a) Distribution of TLR4 and MyD88 proteins in cells and cell membranes. (b,c) The N-terminal, central, and C-terminal domains of TLR4 are divided by the spot line, respectively. (d) The binding position of R/S- baicalin in MYD88. (e) The binding position of R/S- baicalin in TLR4. (f) The binding position of R/S-AS-IV in MYD88. (g) The binding position of R/S-AS-IV in TLR4. (h) The molecular formula of R/Sbaicalin. (i) molecular formula of R/S-AS-IV. (j) the XPS survey of baicalin, TLR4, MyD88, S/R-baicalin +

https://doi.org/10.1021/acs.molpharmaceut.5c00681
Mol. Pharmaceutics 2026, 23, 694−710

Figure 5. continued

TLR4, and S/Rbaicalin + MyD88. j1−j3. C, O, and N element binding energies in baicalin, TLR4, MyD88, S/Rbaicalin + TLR4, and S/R-baicalin + MyD88, respectively. (k) The XPS survey of AS-IV, TLR4, MyD88, S/R-AS-IV + TLR4, and S/R-ASIV + MyD88. k1-k3. C, O, and N element binding energies in AS-IV, TLR4, MyD88, S/RAS-IV + TLR4, and S/R-aAS-IV + MyD88, respectively.

proportion of neutrophils in peripheral blood in the low and high groups was significantly decreased compared with the control group, $P < 0.05$ (Figure 4d) The intensity of Ly6g in tumor tissues was significantly decreased in the high group than the control group, $P < 0.05$. There was no significant difference between the low group and control group, $P > 0.05$ (Figures 4c and S16). Meanwhile, the CD8 + T cells ratio of the three group was 8.55 ± 0.53, 9.84 ± 0.52, and 11.82 ± 0.49, respectively. The proportion of CD8 + T cells in the spleen was significantly increased in the low and high groups compared with the control group, $P < 0.01$(Figure 4d). The expression of CD8 in the high group was elevated than that in the control group ($P < 0.001$), with no difference between low and control groups (Figures 4c and S16). Combined with the above experimental results, we found that dual drugs can effectively reduce neutrophils and increase the proportion of CD8 + T cells in OC mice. Therefore, we hypothesized that dual drugs may inhibit tumor growth by regulating CD8 + T cells and neutrophils. More experiments will be presented for further verification.

RNA-seq was performed to identify differential genes and functional analysis in OC under dual drugs treatment. The total RNA was extracted from tumor tissues, and 16,772 genes were detected. The differential expression results of RNA sequencing showed that 2086 up-regulated genes and 1801 down-regulated genes were detected in the dual drugs group compared with the control group (Figures 4e and S12). The KEGG pathway analysis confirmed the primary biological functions of the differentially expressed genes. Notably, the "PD-L1 expression and PD-1 checkpoint pathway in cancer" (PD-1/PD-L1 signaling pathway) ranked among the top 3 most significantly enriched KEGG pathways, with an enrichment factor (EF) of 0.015 and FDR-adjusted p-values (P_{adj}) of 2.7×10^{-4}. Among them, CD247 and CD274 were significantly increased, while TIRAP, MYD88, HIF1A, IFNGR1, NFKBIB, and other genes were significantly decreased ($P < 0.05$). Considering TIRAP acts as a TLR4 adapter, involved in MyD88-dependent TLR4 signal transduction, it mainly regulates inflammatory signaling pathways to affect the activation, migration, and function of neutrophils. Meanwhile, dual drugs significantly downregulated TLR4/MYD88/NF-κB pathway (EF = 0.021, $P_{adj} = 1.8 \times 10^{-4}$) and neutrophil activation pathways (NOD-like receptor signaling pathway (EF = 0.018, $P_{adj} = 4.2 \times 10^{-3}$). It can be found that dual drugs significantly decrease the TLR4/MYD88/NF-κB pathway protein in OC (Figure S24). Furthermore, we conducted paraffin sections of tumor tissues for MYD88 and Ly6g colocalization staining and found that MYD88 was mainly colocalized with Ly6g, which verified MYD88 expressed on tumor neutrophils, in Figures 4f and S17. It proposed a hypothesis that dual drugs could play an important role in PD-1/PD-L1 signaling pathway by inhibiting TLR4/MYD88/NF-κB pathway of TANs. In the following experiments, we further explored the potential mechanism of dual drugs in OC immunotherapy.

3.4. Binding Affinities and Modes of Interaction between the Drug Candidate and Their Targets

To evaluate the affinity of the candidate drugs for their targets, we performed a molecular docking analysis. The binding poses and interactions of baicalin and AS-IV with two proteins were obtained with Autodock Vina v.1.2.2 and binding energy for each interaction was generated (Figures 5 and Supporting Information S20). Results showed that each candidate bonds to its targets through visible hydrogen bonds and strong electrostatic interactions. Moreover, the hydrophobic pockets of each targets were occupied successfully by the two candidate drugs (Figure 5d−g and S19 and S20). For baicalin, TLR4 and MYD88 had low binding energies of −8.701 and −7.418 kcal/mol, indicating high stable binding. For AS-IV, TLR4 and MYD88 had low binding energies of −9.503 and −7.27 kcal/mol, indicating high stable binding (Tables 2 and S2).

Table 2. Binding Energy

target	drug	binding Energy (kcal/mol)
TLR4	baicalin	−8.701
MYD88	baicalin	−7.418
TLR4	AS-IV	−9.503
MYD88	AS-IV	−7.27

Meanwhile, the different positions of baicalin and AS−IV interaction with TLR4 are shown in Figure 5a−c, respectively. Therein, the binding position of baicalin present at the transmembrane region of the TLR4 structure increases binding to the envelope to fix the receptor, and the binding position of AS-IV present at intercellular region of TLR4 structure enhances the guidance of the interaction and forms a signal complex. In contrast, the binding positions of baicalin and AS-IV in MyD88 are the same (Figures 5a and S20) and at the C-terminus of the MyD88 structure. The C-terminals of MyD88 and TLR4 structures bind together to mediate downstream signaling. Therefore, baicalin and AS-IV which induce or reduce other adaptor proteins were recruited by intracellular cascade reaction. Besides, baicalin and AS-IV interact with TLR4 and Myd88 which have been confirmed by X-ray photoelectron spectroscopy (XPS), and the combination acts as the TLR4 inhibitor on the PD-1/PD-L1 immune response due to overlapping binding sites (Figure 5j,k, S21 and S22)

To verify the results of the molecular dynamics simulations, we analyze baicalin and AS-IV interactions with TLR4 and Myd88 by XPS. In Figure 5j−k3, we observe that the intensity of C═O, C−OR, and C 1s would be changed when baicalin and AS-IV interact with TLR4 and MyD88. Therein, the baicalin interacts with Myd88 causing the intensity of C−OR to be increased and interacts with TLR4 causing the intensity of C═O to be decreased (Figure 5j−3). In Figure 5k−k3, when baicalin interacts with TLR4, the MgO of TLR4 has vanished, and the intensity of O 1s and B2O3 of MyD88 is increased, respectively. Meanwhile, the intensity H4 has appeared in TLR4 when baicalin interacts with TLR4, and N 1s has been vanished. The same analysis can be observed when AS-IV interacts with TLR4 and MyD88. The intensity of C═O has been decreased

https://doi.org/10.1021/acs.molpharmaceut.5c00681
Mol. Pharmaceutics 2026, 23, 694−710

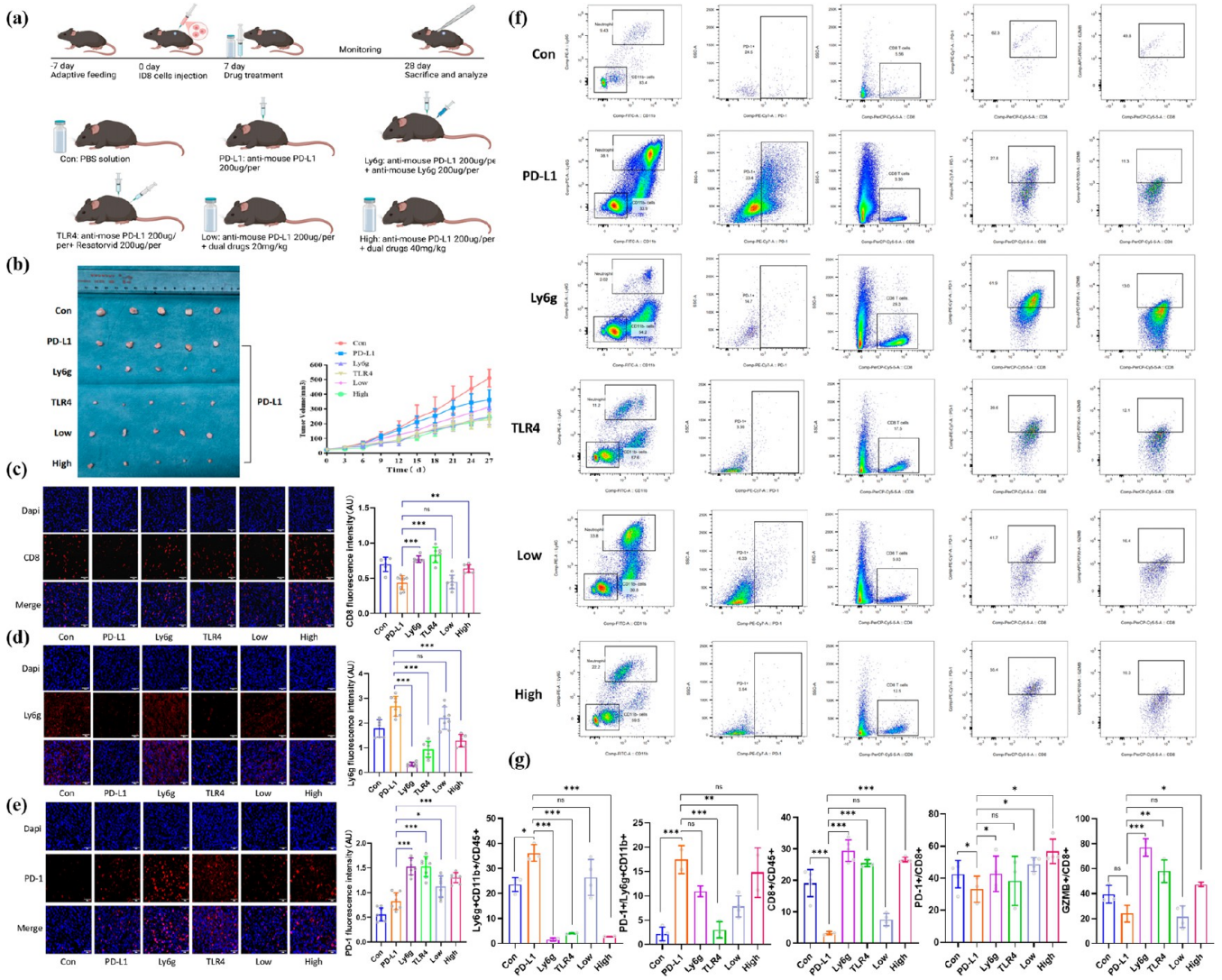

Figure 6. Tumor growth in C57 mice treated with different drugs, detection of neutrophils, and CD8 + T cells in the tumor of C57 mice treated with different drugs. (a) Illusion of mice models (b) Subcutaneous tumor and tumor growth curves of C57 mice treated with different drugs. (c−e) The intensity of Ly6g, CD8, and PD-1 in tumor tissues detected by immunofluorescence under different drug concentrations (magnification × 400), and statistical data. (f) The proportion of Ly6g + CD11b+, PD-1 + Ly6g + CD11b+, CD8+, GZMB + CD8+, and PD-1 + CD8+ cells of C57 mice by flow cytometry. (g) Quantitative statistics of f.*$P < 0.05$, **$P < 0.01$, ***$P < 0.001$, and ns had no statistical difference.

when AS-IV interacts with MyD88, and on the contrary, the intensity of C═O has been increased when AS-IV interacts with TLR4. Therefore, baicalin and ASIV interact with TLR4 and Myd88 which have been confirmed by XPS.

3.5. Dual Drugs Reduce the TLR4/MYD88/NF-κB Pathway Regulated by Tumor Associated Neutrophils to Increase the CD8+T Cell Immune Response in the PD-1/PD-L1 Pathway

In our study, we found that there was a significant decrease in neutrophils and a remarkable increase in CD8 + T cells under the administration of dual drugs; therefore, we inferred that dual drugs reduced the neutrophils of OC and increased the CD8 + T cell immune response by regulating the TLR4/MYD88/NF-κB pathway. We designed an experiment in six groups to verify this hypothesis. ID8 cell suspension was transplanted subcutaneously in C57 mice and randomly divided into six groups: control group, PD-L1 group, Ly6g group, TLR4 group, low group, and high group (Figure 6a and Section S3 Mice tumor model ⑤).

As shown in Figures 6b and S11, tumors of the PD-L1 group were smaller than those in the control group ($P < 0.001$). The tumor of Ly6g and the TLR4 group was smaller than that of the PD-L1 group ($P < 0.001$), and the tumor of the high group was significantly reduced ($P < 0.01$), with no significant difference to the Ly6g and the TLR4 group, $P > 0.05$. It can be found that the dual drugs can effectively enhance the inhibitory treatment of the PD-L1 antibody in OC. Moreover, the results show that dual drugs induced immunofluorescence expression of neutrophils in C57 mice. The Ly6g expression in the PD-L1 group was significantly higher than that in the control group, $P < 0.05$; The expression of Ly6g, TLR4, and the high group was lower than that of the PD-L1 group ($P < 0.001$) (Figures 6c and S18). The CD8 expression in the PD-L1 group was significantly lower than that in the control group ($P < 0.05$); The expression of Ly6g, TLR4, and the high group was higher than that of the PD-L1 group ($P < 0.01$) (Figures 6d and S18). The PD-1 expression of Ly6g, TLR4, and low and high groups was higher than that of the PD-L1 group ($P < 0.05$) (Figures 6e and S18). Results showed that PD-L1 blocking therapy could increase the expression of

https://doi.org/10.1021/acs.molpharmaceut.5c00681
Mol. Pharmaceutics 2026, 23, 694−710

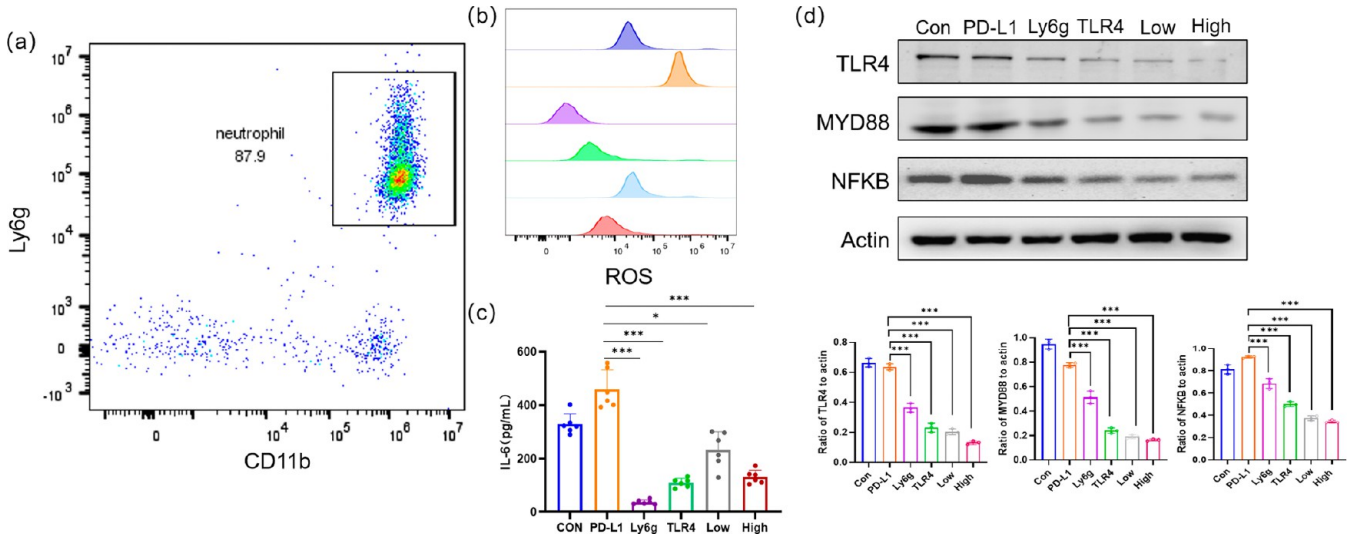

Figure 7. TAN depletion functional assays and protein expression of TLR4/MYD88/NF-κB axis (a) Purity of TAN. (b) ROS detection of TAN. (c) IL-6 detection of TAN. (d) Protein levels of TLR4/MYD88/NF-κB axis in TAN. (e) Quantitative statistics of *D*. *$P < 0.05$, ***$P < 0.001$.

Ly6g and weaken the fluorescence intensity of CD8 in tumor tissues, while dual drugs could reduce the expression of Ly6g and increase the expression of CD8 and PD-1 in tumors.

In addition, after the tumors were resected, flow cytometric analysis of neutrophils and T cells were performed. As a result, the proportions of Ly6g + CD11b+ in six groups were 23.60 ± 2.77, 36.17 ± 3.35, 1.52 ± 0.63, 4.07 ± 0.19, 26.44 ± 7.16, and 2.82 ± 0.08. The proportion of neutrophils in the PD-L1 group was significantly higher than that in the control group ($P < 0.05$); the proportion of neutrophils in Ly6g, TLR4, and the high group was significantly lower than that in the PD-L1 group($P < 0.001$). Meanwhile, the proportions of PD-1 + Ly6g + CD11b+ in six groups were 2.20 ± 1.41, 17.45 ± 2.88, 10.92 ± 1.10, 3.03 ± 1.69, 7.85 ± 2.17, and 14.80 ± 5.10, respectively. The proportion of PD-1 + Ly6g + CD11b+ in the PD-L1 group was significantly higher than the control group ($P < 0.001$); The proportion of TLR4 and the low group was significantly lower than the PD-L1 group ($P < 0.01$). Statistically, the proportions of CD8 + T cells in tumors of mice were 19.12 ± 4.29, 3.21 ± 0.54, 29.43 ± 3.45, 25.50 ± 1.09, 7.54 ± 1.91, and 26.60 ± 0.76. The proportion of the PD-L1 group was significantly lower than the control group ($P < 0.001$); The proportion of Ly6g, TLR4, and the high group was significantly higher than that in the PD-L1 group($P < 0.001$). At the same time, the proportion of PD-1 + CD8 + T cells was 42.55 ± 8.52,33.14 ± 8.09,42.79 ± 11.06,38.37 ± 15.25,48.58 ± 4.27, and 56.78 ± 7.63. The proportion of the PD-L1 group was significantly lower than the control group ($P < 0.05$); The proportion of Ly6g, low and high groups was significantly higher than that in the PD-L1 group ($P < 0.05$). The proportion of GZMB + CD8+ was 39.51 ± 7.10, 24.01 ± 6.69, 76.95 ± 7.00, 57.93 ± 9.12, 21.54 ± 8.71, and 47.40 ± 1.70. The proportion of Ly6g, TLR4, and the high group was significantly higher than the PD-L1 group ($P < 0.05$). Furthermore, dual drugs reduced neutrophils and elevated CD8 + T cells in spleen and peripheral blood, while increasing both neutrophils and CD8+T cells of bone marrow cells (Figures S13−S15). It was found that the combination of dual drugs could decrease TANs, upregulate the ratio of CD8 + T cells, and increase GZMB + T cells and PD-1 + T cells in the tumor.

3.6. Dual Drugs Downregulate ROS and IL-6 in Tumor Associated Neutrophils via the TLR4/MYD88/NF-κB Pathway

Furthermore, we extracted the neutrophils from the tumor by the neutrophil enrichment kit (stemcell, 19762) and then conducted the detection of ROS by reactive oxygen species assay kit (beyotime, S0033S) and IL-6 (beyotime, PY2782). The purity of TAN was over 80% (Figures 7a and S25), and the ROS concentration in Ly6g, TLR4, and high groups significantly decreased compared with the PD-L1 group ($P < 0.001$), while the low group showed a decrease compared with the PD-L1 group ($P < 0.01$). Meanwhile, the IL-6 levels in the Ly6g, TLR4, and high groups significantly decreased compared with the PD-L1 group ($P < 0.001$), and the low group exhibited a decrease compared with the PD-L1 group ($P < 0.05$) (Figure 7b,c and S25). In addition, we extracted proteins from neutrophils in tumor tissues and conducted Western blotting experiments to verify the gene expression. As shown in Figure 7d,e, TLR4, MYD88, and NF-κB protein levels in Ly6g, TLR4, low and high groups significantly decreased compared to the PD-L1 group ($P < 0.05$). In conclusion, dual drugs increase TAN depletion in TLR4/MYD88/NF-κB manner.

3.7. Dual Drugs Decrease the TLR4/MYD88/NF-κB Pathway and Cause No Adverse Events

Besides, we performed immunohistochemical staining on tumor tissues. In Figures 8a−d and S23, compared with the control group, the expression of TLR4 was higher in the PD-L1 group ($P < 0.05$); the score of Ly6g, TLR4 and the high group was lower than the PD-L1 group ($P < 0.001$). Besides, the expression of MYD88 in the PD-L1 group was higher than the control group ($P < 0.05$); the score of Ly6g, TLR4, low and high groups was lower than the PD-L1 group ($P < 0.01$). What is more, the expression of NF-κB in the PD-L1 group was higher than in the control group ($P < 0.05$); the score of Ly6g, TLR4, and the high group was lower than the PD-L1 group ($P < 0.001$). Comparing the expression of PD-L1 in IHC tissues, we found that there was no significant difference between the PD-L1 group and the control group ($P > 0.05$). The score of Ly6g and the high group was higher than that of the PD-L1 group ($P < 0.001$). It implied that dual drugs can increase the expression of PD-L1 in tumor tissues treated with PD-L1 blocker. It reveals that the dual drugs

https://doi.org/10.1021/acs.molpharmaceut.5c00681
Mol. Pharmaceutics 2026, 23, 694−710

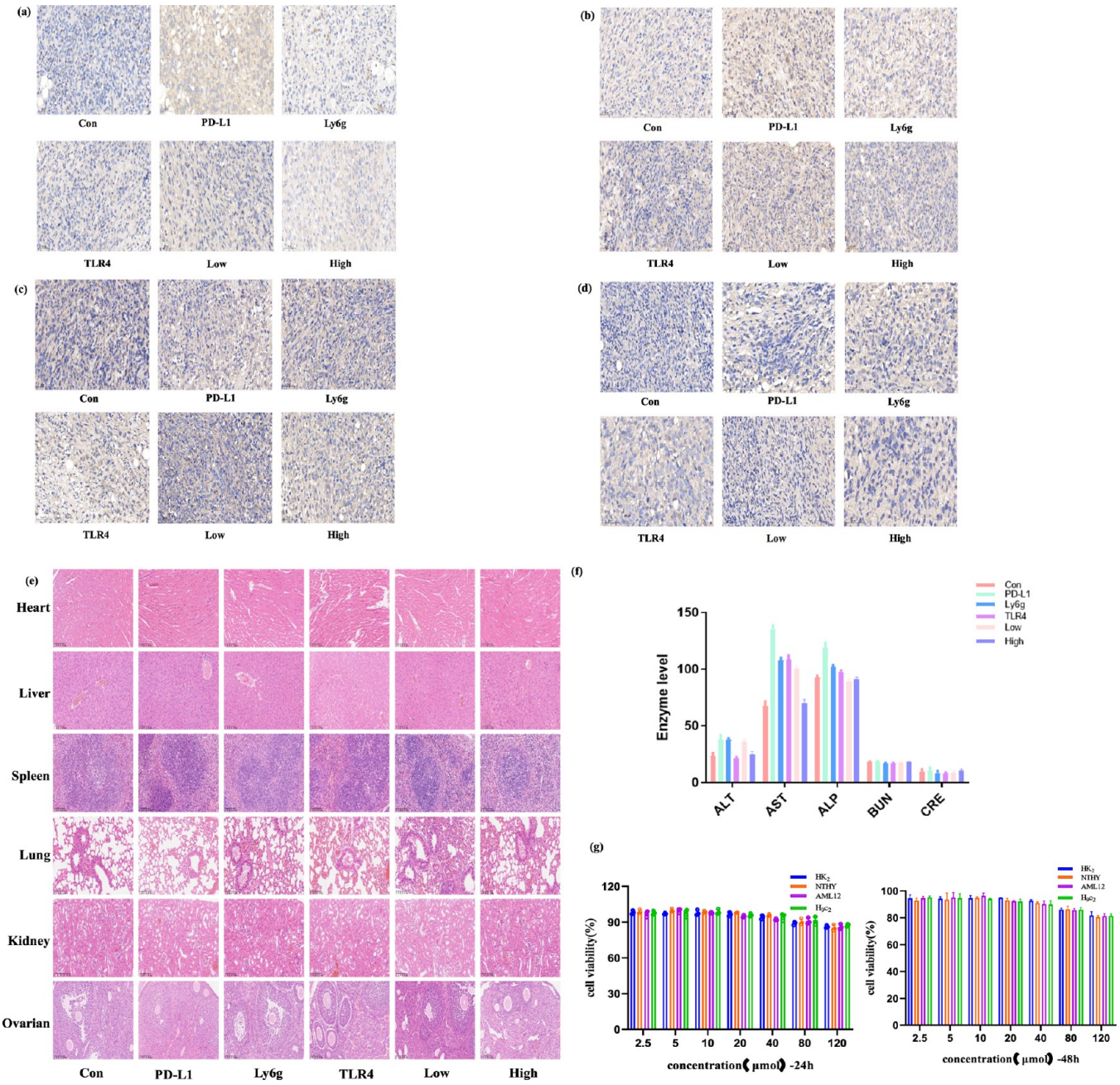

Figure 8. Immunohistochemical detection of TLR4, MYD88, NF-κB, and PD-L1 in tumors of C57 mice treated with different drugs and side effect evaluation (magnification × 400). (a) The contents of TLR4 in C57 mice treated with different drugs and quantitative statistics. (b) The contents of MYD88 in C57 mice treated with different drugs and quantitative statistics. (c) The contents of NF-κB in C57 mice treated with different drugs and quantitative statistics. (d) The contents of PD-L1 in C57 mice treated with different drugs and quantitative statistics. (e) Hematoxylin and Eosin staining of major organs (heart, liver, spleen, lung, kidney, and ovarian) in different groups. (f) Liver and kidney biochemical indexes of C57 mice in different groups. (g) Cell viabilities of liver, kidney, thyroid, and myocardial normal cell lines under different concentrations. $^{*}P < 0.05$, $^{**}P < 0.01$, ns showed no statistical difference.

inhibit the TLR4/MYD88/NF-κB pathway to reduce TANs-derived ROS/IL-6, which in turn increases PD-L1 expression and restores CD8+ T cell activity.

In addition, we removed main organs like heart, liver, spleen, lung, kidney, and ovary to perform HE staining and found no significant difference in morphology among all groups. Meanwhile, there was no significant difference between groups in liver and kidney biochemical indexes, while the normal cell viabilities were maintained over 80% after incubating at the concentration of 120 μm for 24 and 48 h, which indicated dual drugs exhibited no significant toxic effects on normal cells and organs at the therapeutic concentration(Figures 8e,f and S23).

4. DISCUSSION

According to the 2020 edition of the histological classification (developed by the World Health Organization), ovarian tumors include 13 broad categories of pathological types, and EOC) are the most common histological type, accounting for 50%−70% cases. As the seventh most common disease in female cancer, its 5 year survival rate after diagnosis is only 30−51%. An important

https://doi.org/10.1021/acs.molpharmaceut.5c00681
Mol. Pharmaceutics 2026, 23, 694−710

factor behind the low survival rate is that patients are often found to be in the advanced stage when diagnosed.[18−21] In contrast, when OC is diagnosed at an early stage, the 5 year survival rate is often 92%, but when the disease reaches an advanced stage, this indicator is as low as 29%.[1] What is more, due to its hidden clinical symptoms in the early and middle stages, three-quarters of patients are not diagnosed during a visit until they have reached an advanced stage of the disease. The current treatment mode for OC is surgery/neoadjuvant chemotherapy + surgery, postoperative adjuvant chemotherapy, maintenance therapy, and relapse after initial treatment. According to statistics, the overall effective rate of carboplatin combined with the paclitaxel (TC) regimen, as traditional first-line chemotherapy regimens for OC, is about 30%−40%. If drug resistance develops, then the standard first-line chemotherapy regimen becomes ineffective. For patients with recurrent OC, the objective response rate to second-line treatment regimens (recommended by the NCCN Guidelines) is typically only 5%−20%, leaving these patients in a dilemma of having almost no effective therapeutic options.[22] Therefore, it is an urgent problem for gynecologic oncologists to improve the therapeutic effect of OC and reduce tumor recurrence.

Recent clinical trials have shown that PD-1/PD-L1 blocking therapy has shown unprecedented lasting efficacy in patients with various cancers.[4,9] However, only a small number of patients could benefit from it due to immune ignorance with little or no tumor infiltrating immune cell infiltration, immune cell infiltration within nonfunctional immunity, such as little or no expression of PD-L1, or immune infiltration present only at the outer edge of the tumor cell mass.[23] In order to improve the response rate, many scholars continue to explore the field of ICB combination drug research, and a number of clinical trials of combined blocking of CTLA4 and PD-1/PD-L1 have shown lasting survival benefits for various tumor types.[24−26] The combination of ICBs with chemotherapy drugs is thought to kill immunosuppressive cells in TME while increasing exposure to tumor antigens by inducing tumor cell death, thereby enhancing the host immune system's recognition and elimination of tumor cells.[9] To this end, ICBs in combination with concurrent and/or chemotherapy are being extensively studied, with phase III clinical data showing benefits in OS and/or progression-free survival in patients with nonsmall cell lung cancer,[27−29] triple-negative breast cancer,[30] and head and neck squamous cell carcinoma.[31] Similarly, the combination of ICBs and targeted therapies has also improved clinical responses in liver and endometrial cancer.[32−34] However, the effect of different chemotherapy agents on the immune response in TME has not been fully elucidated, and the risk of immune-related adverse events (irAE) in immune-related adverse cases is significantly increased if patients are given a combination medication strategy. Any organ can be affected by irAE, with the skin, gastrointestinal tract, and endocrine system (including the thyroid, adrenal, and pituitary glands) most likely to be involved, with effects ranging from mild to fatal.[35] Based on the above background, it is urgent to find a drug combined with ICB to enhance therapeutic efficacy while reducing adverse events.

OC is mainly infiltrated by dysfunctional T cells and immunosuppressive Treg cells, so it is defined as the immune "cold" mode.[6] Immunotherapy for OC has long been neglected, but some studies suggest that some OC patients can still benefit from immune checkpoint inhibitors. Therefore, the relationship between PD-1/PD-L1 expression in OC and the TME needs to be further investigated. The PD-1/PD-L1 signaling pathway plays an important role in tumor evasion of host immune response, and numerous studies have shown that it is directly related to the prognosis of various cancers.[3,36,37] Our sequencing found that dual drugs are enriched in the PD-1/PD-L1 pathway, suggesting that dual drugs may improve the outcome of OC patients through immune regulation. High expression of PD-L1 on tumor cells associates with better immune response to immune checkpoint blockade, while many studies found that patients with negative expression of PD-L1 in tumors could still benefit from immunotherapy. Therefore, PD-L1 expression seems not a static feature but a dynamic feature that changes with time and treatment. Some scholars even believe that ICB efficacy is not related to PD-L1 expression in tumor tissues but to tumor immune microenvironment, in which T cell infiltration plays a very important role.[6,38] Clonal analysis has found that anti-PD-1 treatment affects the evolutionary landscape of patients' tumors and may lead to clonal expansion of certain T cells. In patients with advance disease, T cells are mainly represented by selective expansion of regulatory T cells with ineffective response or immunosuppression.[39] By establishing a mouse model of OC, we found that the density of CD8 + T cells in the tumor and spleen increased significantly when the mice received baicalin-AS-IV combination treatment. Therefore, we hope to further explore the mechanism of the combination of dual drugs in the immune microenvironment of OC. The aim is to find a new treatment to transform the state of T cell depletion into a cytotoxic clone subgroup and improve the immune response to ICB therapy.

As the most abundant immune cells in the human body, neutrophils infiltrate all parts of the human body. In the TME, the view that neutrophils are only a bystander has been overturned. Studies have shown that in patients with disease progression, there is a large number of neutrophils infiltrated in tumor tissues, or a large accumulation of neutrophils in peripheral blood or an increased ratio of neutrophils to lymphocytes in peripheral blood.[40,41] Multiple studies have shown that in the case of hypoxia, the essence creates a special inflammatory environment to recruit white blood cells, in which neutrophils may produce harm to the body due to the antimicrobial and immunomodulatory mediators such as MMPs, ROS, and VEGF produced by MMPS, changing the immune microenvironment while promoting the occurrence, development, angiogenesis, progression, and metastasis.[42,43] Gentles et al. created a new resource (PRECOG) to analyze the relationship between clinical outcomes and the abundance of multiple tumor-associated white blood cell (TAL) subpopulations. This large-scale global genetic analysis confirmed that neutrophils are the primary immune prognostic parameter of cancer and suggested that neutrophils may influence prognosis through interaction with other immune cells.[42] In TME, TAN is closely related to other immune cells, and neutrophils should be a key mediator in the efficacy, clinical value, and toxicity of these treatments in patients treated with ICB. High TAN density predicted poor OS, while high infiltration of CD8 + GZMB + T cells was positively correlated with survival.[8,44] In gastric cancer, the release of GM−CSF induces the activation of neutrophils within the tumor, which is accompanied by the activation of JAK/STAT3 signaling pathway and induces the expression of PD-L1.[45] These activated neutrophils exert their tumor-promoting role by inhibiting T cell immunity in a PD-1/PD-L1-dependent manner, promoting immunosuppression and disease progression.[46] In our works, we found that CD8 + T cells proliferated after anti-PD-L1 treatment but mainly depleted

https://doi.org/10.1021/acs.molpharmaceut.5c00681
Mol. Pharmaceutics 2026, 23, 694−710

PD-1 + CD8 + T cells, which is consistent with existing research results.[6,39] In addition, after receiving Ly6g inhibitor, neutrophils in spleen, peripheral blood and tumor tissues were significantly inhibited, and bone marrow cells produced a large number of naive neutrophils. Meanwhile, CD8 + T cells were significantly increased, and GZMB + T cells with a killing effect were mainly increased, while the proportion of depleted PD-1 + T cells was significantly reduced. Therefore, neutrophils in the immune microenvironment can reduce the expansion of cytotoxic CD8 + T cells and increase their depletion in tumor therapy; however, Ly6g inhibitors may inhibit neutrophils, which are responsible for killing pathogens and exerting anti-infective effects, thereby increasing the risk of infection in patients, so that we need milder alternative drugs.

Baicalin, a flavonoid isolated from the *Scutellaria baicalensis* plant, is a potential anticancer candidate that can inhibit tumor growth, induce cell death, and inhibit metastasis in various cancers. At the same time, as a novel therapeutic drug that can target TLR4, baicalin combines with TLR4 to inhibit the TLR4/HIF-1α/VEGF pathway in colorectal cancer.[9] AS-IV is a saponin compound isolated from Astragaloside, which can play a role in antitumor activities by regulating the TME and tumor cell growth cycle. AS-IV inhibits the proliferation, invasion, and migration of tumor cells by regulating TLR4/NF-κB/STAT3 signaling pathway or inhibiting macrophage M2 polarization by the HMGB1-TLR4 axis.[9,16,47] In tumors, neutrophils can inhibit the T cell immune response through the PD-1/PD-L1 pathway, thus achieving immune escape.[39] Since TLR4 is an inflammatory sensor that is highly expressed on TAN,[48] baicalin and AS-IV have been reported in multiple literature to target TLR4 for antitumor effects.[9,16] Sequencing results analyzed the involvement of baicalin and AS-IV in the PD-1/PD-L1 pathway through the TLR4/MYD88/NF-κb pathway, which is a classical inflammatory pathway. The TOLL receptor family is expressed in myeloid cells, and most of the genes highly related to myeloid phenotypes are involved in the recruitment and function of neutrophil lineages. The toll-IL-1 receptor (TIR) domain containing aptamectin (TIRAP) and IL1R2, encodes innate and IL-1β signaling proteins that promote rich inflammatory responses in bone marrow cells, was decreased in dual drug treated cells and mice.[49] The TLR4/MYD88 pathway is an essential pathway for encoding antitumor neutrophils.[50] Studies have found that in endometrial cancer, TAN mainly changes the structure of the tumor cell $\alpha 6\beta 4$ binding complex through the MYD88 pathway to promote tumor cell shedding.[50] MYD88, as a TLR-4 signal transduction protein, is an important downstream component of the TLRs signal cascade, which can mediate the paclitaxel resistance of EOC and is not expressed in normal ovaries. Studies have shown that positive expression of MYD88 is significantly correlated with tumor metastasis, disease-free survival and OS, that is, positive expression of MYD88 is a significant adverse prognostic factor for EOC.[51] Our experimental results showed that ICB with TLR4 inhibitors significantly inhibited tumor growth by inhibiting the TLR4/MYD88/NF-κb pathway and improved the killing effect of CD8 + T cells. As a natural TLR4 inhibitor, baicalin-AS-IV targets the TLR4/MYD88 dual complex, with a stronger inhibitory effect on the TLR4/MYD88/NF-κb pathway of neutrophils and a minor inhibitory effect on peripheral blood, spleen, and bone marrow. Combined with the above analysis and our experimental results, we concluded that a dual drug can increase the killing effect of CD8 + T cells by inhibiting the TLR4/MYD88/NF-κb pathway of TANs in OC.

It is believed that neutrophils can be divided into pro-tumor type N1 and antitumor type N2, or seven types of N1−N6, each of which has different mechanisms of action in the field of tumor.[41] In addition, neutrophils are indistinguishably defined from bone marine-derived suppressor cells (MDSC), which express high levels of CD11b, arginase, and granulocyte marker GR1, which is composed of the membrane proteins Ly6c and Ly6g. They can be broadly divided into monocytes (CD11b + Ly6G-Ly6C$_{high}$) and polymorphonuclear (CD11b + Ly6G + Ly6C$_{low}$) groups, the latter being the dominant group in most cancers.[52] All in all, MDSC and neutrophils may play different or even opposite roles in biology, but there is no clear criterion to distinguish these two. Thus, this represents an area requiring further investigation. Not only does the presence of neutrophils themselves influence the immune response but their specific location in the tumor may also be associated with prognosis. Unlike peri-tumor or stromal neutrophils, intratumor neutrophils have the strongest association with a poor prognosis. In addition, circulating neutrophils can coordinate with the TAN to promote tumor growth, invasion, and even tumor-associated thrombosis by releasing neutrophilic extracellular traps. Recent high-dimensional single-cell analyses have shown that circulating and tumor-infiltrating neutrophils exhibit heterogeneity in their transcriptome and surface protein expression levels. This brings a new direction for future research, that is, whether the phenotypically different neutrophil states that coexist in tumors have different origins or different functional activities, and whether specific antitumor states can be expanded therapeutically.[41]

5. CONCLUSION

Combined with the above experimental results, we found that the combination of R-baicalin and R-AS-IV acted on the PD-1/PD-L1 signaling pathway in OC, which was consistent with the results of our studies and reflected our idea of combining traditional Chinese and Western medicine to improve body immunity. It was further found that the combination of R-phenotype chiral of dual drugs could reduce TANs, enhance TAN depletion by decreasing ROS and IL-6, increase the density of GZMB + CD8 + T cells, and reduce the depletion of PD-1 + CD8 + T cells, while high infiltration of GZMB + CD8 + T cells was associated with a better prognosis. Therefore, the dual drug has the effect of reducing TANs and increasing the cytokilling of CD8+T cells in OC. In summary, R-baicalin-AS-IV plays an antitumor role by reducing TAN recruitment to inhibit the TLR4/MYD88/NF-κB signaling pathway and enhance CD8+T cell immune killing.

■ ASSOCIATED CONTENT

Data Availability Statement

The data that support the findings of this study are available from the corresponding author upon reasonable request.

Supporting Information

The Supporting Information is available free of charge at https://pubs.acs.org/doi/10.1021/acs.molpharmaceut.5c00681.

Double metal cladding waveguide cavity; in vitro and in vivo experiments; RNA sequencing analysis; PBMC extraction and immune cell subsets; molecular docking data with XPS verification; side effects of dual drugs; qRT-PCR primer sequences and results; and TAN isolation

https://doi.org/10.1021/acs.molpharmaceut.5c00681
Mol. Pharmaceutics 2026, 23, 694−710

and functional detection such as the ROS and IL-6 assays (PDF)

AUTHOR INFORMATION

Corresponding Authors

Hailang Dai − *Department of Traditional Chinese Medicine, Department of Head and Neck Surgery, Renji Hospital, School of Medicine, School of Physics and Astronomy, Shanghai Jiao Tong University, Shanghai 200127, China; State Key Laboratory of Advanced Optical Communication Systems and Networks, Shanghai Jiao Tong University, Shanghai 200240, China;* orcid.org/0000-0002-1301-7448; Email: hailangdai@sjtu.edu.cn

Xianfeng Chen − *Department of Traditional Chinese Medicine, Department of Head and Neck Surgery, Renji Hospital, School of Medicine, School of Physics and Astronomy, Shanghai Jiao Tong University, Shanghai 200127, China; State Key Laboratory of Advanced Optical Communication Systems and Networks, Shanghai Jiao Tong University, Shanghai 200240, China; Collaborative Innovation Center of Light Manipulations and Applications, Shandong Normal University, Jinan 250358, China*; Email: xfchen@sjtu.edu.cn

He Li − *Department of Traditional Chinese Medicine, Department of Head and Neck Surgery, Renji Hospital, School of Medicine, School of Physics and Astronomy, Shanghai Jiao Tong University, Shanghai 200127, China;* orcid.org/0000-0002-3630-0975; Email: lihe1972@hotmail.com

Authors

Yi Lai − *Department of Traditional Chinese Medicine, Department of Head and Neck Surgery, Renji Hospital, School of Medicine, School of Physics and Astronomy, Shanghai Jiao Tong University, Shanghai 200127, China*

Dan Ru − *Department of Traditional Chinese Medicine, Department of Head and Neck Surgery, Renji Hospital, School of Medicine, School of Physics and Astronomy, Shanghai Jiao Tong University, Shanghai 200127, China*

Chenhuan Ding − *Department of Traditional Chinese Medicine, Department of Head and Neck Surgery, Renji Hospital, School of Medicine, School of Physics and Astronomy, Shanghai Jiao Tong University, Shanghai 200127, China*

Ling Ding − *Department of Traditional Chinese Medicine, Department of Head and Neck Surgery, Renji Hospital, School of Medicine, School of Physics and Astronomy, Shanghai Jiao Tong University, Shanghai 200127, China*

Chen Wang − *Department of Traditional Chinese Medicine, Department of Head and Neck Surgery, Renji Hospital, School of Medicine, School of Physics and Astronomy, Shanghai Jiao Tong University, Shanghai 200127, China*

Cenxin Luo − *Department of Traditional Chinese Medicine, Department of Head and Neck Surgery, Renji Hospital, School of Medicine, School of Physics and Astronomy, Shanghai Jiao Tong University, Shanghai 200127, China*

Yujie Qi − *Department of Traditional Chinese Medicine, Department of Head and Neck Surgery, Renji Hospital, School of Medicine, School of Physics and Astronomy, Shanghai Jiao Tong University, Shanghai 200127, China; State Key Laboratory of Advanced Optical Communication Systems and Networks, Shanghai Jiao Tong University, Shanghai 200240, China*

Complete contact information is available at: https://pubs.acs.org/10.1021/acs.molpharmaceut.5c00681

Author Contributions

[‖]Y.L., D.R. and H.D. are contributed equally to this work.

Notes

The authors declare no competing financial interest.

ACKNOWLEDGMENTS

This work was supported by the Medical and Industrial Cross Project of Shanghai Jiaotong University (No. YG2023QNB08), Shanghai Municipal Health Commission Health industry clinical research project (No. 20234Y0089), Shanghai Health Commission Traditional Chinese Medicine research project (No. 2022QN068), the National Natural Science Foundation of China (NSFC) (No. 12574361, 82374163, 82174135, 82574758 and 12192252), the Shanghai Municipal Science and Technology Major Project (Grant No. 2019SHZDZX01-06), Medical innovation research Project of Science and Technology Innovation Action Plan of Shanghai Municipal Science and Technology Commission (No. 21Y21920503) and Natural Science Foundation of Shanghai (No. 23ZR1428400).

REFERENCES

(1) Ferlay, J.; Soerjomataram, I.; Dikshit, R.; Eser, S.; Mathers, C.; Rebelo, M.; Parkin, D. M.; Forman, D.; Bray, F. Cancer incidence and mortality worldwide: sources, methods and major patterns in GLOBOCAN 2012. *Int. J. Cancer* **2015**, *136* (5), E359−E386.

(2) Siegel, R. L.; Giaquinto, A. N.; Jemal, A. Cancer statistics, 2024. *CA Cancer J. Clin.* **2024**, *74* (1), 12−49.

(3) Zou, W.; Wolchok, J. D.; Chen, L. PD-L1 (B7-H1) and PD-1 pathway blockade for cancer therapy: Mechanisms, response biomarkers, and combinations. *Sci. Transl. Med.* **2016**, *8* (328), 328rv4.

(4) Lei, X.; Lei, Y.; Li, J. K.; et al. Immune cells within the tumor microenvironment: Biological functions and roles in cancer immunotherapy. *Cancer Lett.* **2020**, *470*, 126−133.

(5) Tumeh, P. C.; Harview, C. L.; Yearley, J. H.; et al. PD-1 blockade induces responses by inhibiting adaptive immune resistance. *Nature* **2014**, *515* (7528), 568−571.

(6) Lin, H.; Wei, S.; Hurt, E. M.; et al. Host expression of PD-L1 determines efficacy of PD-L1 pathway blockade-mediated tumor regression. *J. Clin. Invest.* **2018**, *128* (2), 805−815.

(7) Yang, B.; Li, X.; Zhang, W.; et al. Spatial heterogeneity of infiltrating T cells in high-grade serous ovarian cancer revealed by multi-omics analysis. *Cell Rep. Med.* **2022**, *3* (12), 100856.

(8) Ponzetta, A.; Carriero, R.; Carnevale, S.; et al. Neutrophils Driving Unconventional T Cells Mediate Resistance against Murine Sarcomas and Selected Human Tumors. *Cell* **2019**, *178* (2), 346−360.

(9) Li, K.; Tandurella, J. A.; Gai, J.; et al. Multi-omic analyses of changes in the tumor microenvironment of pancreatic adenocarcinoma following neoadjuvant treatment with anti-PD-1 therapy. *Cancer Cell* **2022**, *40* (11), 1374−1391.

(10) Zhao, Q.; Chen, X. Y.; Martin, C. Scutellaria baicalensis, the golden herb from the garden of Chinese medicinal plants. *Sci. Bull.* **2016**, *61* (18), 1391−1398.

(11) Jia, L.; Lv, d.; Zhang, S.; Wang, Z.; Zhou, B. Astragaloside IV inhibits the progression of non-small cell lung cancer through the Akt/GSK-3β/β-catenin pathway. *Oncol. Res.* **2019**, *27*, 503−508.

(12) Jia, L.; Lv, D.; Zhang, S.; Wang, Z.; Zhou, B. Astragaloside IV Inhibits the Progression of Non-Small Cell Lung Cancer Through the Akt/GSK-3β/β-Catenin Pathway. *Oncol Res.* **2019**, *27* (4), 503−508.

(13) Wang, X.; Gao, S.; Song, L.; Liu, M.; Sun, Z.; Liu, J. Astragaloside IV antagonizes M2 phenotype macrophage polarization-evoked ovarian cancer cell malignant progression by suppressing the HMGB1-TLR4 axis. *Mol. Immunol.* **2021**, *130*, 113−121.

(14) Liang, Y.; Chen, B.; Liang, D.; et al. Pharmacological Effects of Astragaloside IV: A Review. *Molecules* **2023**, *28* (16), 6118.

(15) Chen, M.; Zhong, K.; Tan, J.; Meng, M.; Liu, C. M.; Chen, B.; Huang, C.; Wong, H. L. X.; Bian, Z.; Su, T.; et al. Baicalein is a novel

TLR4-targeting therapeutics agent that inhibits TLR4/HIF-1α/VEGF signaling pathway in colorectal cancer. *Clin. Transl. Med.* **2021**, *11* (11), No. e564.
(16) Wang, X.; Gao, S.; Song, L.; Liu, M.; Sun, Z.; Liu, J. Astragaloside IV antagonizes M2 phenotype macrophage polarization-evoked ovarian cancer cell malignant progression by suppressing the HMGB1-TLR4 axis. *Mol. Immunol.* **2021**, *130*, 113−121.
(17) Ziyang, T.; Xirong, H.; Chongming, A.; Tingxin, L. The potential molecular pathways of Astragaloside-IV in colorectal cancer: A systematic review. *Biomed. Pharmacother.* **2023**, *167*, 115625.
(18) Sung, H.; Ferlay, J.; Siegel, R. L.; et al. Global Cancer Statistics 2020: GLOBOCAN Estimates of Incidence and Mortality Worldwide for 36 Cancers in 185 Countries. *CA Cancer J. Clin.* **2021**, *71* (3), 209−249.
(19) Torre, L. A.; Trabert, B.; DeSantis, C. E.; et al. Ovarian cancer statistics, 2018. *CA Cancer J. Clin.* **2018**, *68* (4), 284−296.
(20) Lheureux, S.; Gourley, C.; Vergote, I.; Oza, A. M. Epithelial ovarian cancer. *Lancet* **2019**, *393* (10177), 1240−1253.
(21) Kawka, E.; Witowski, J.; Sandoval, P.; et al. Epithelial-to-Mesenchymal Transition and Migration of Human Peritoneal Mesothelial Cells Undergoing Senescence. *Perit. Dial. Int.* **2019**, *39* (1), 35−41.
(22) Armstrong, D. K.; Alvarez, R. D.; Bakkum-Gamez, J. N.; et al. Ovarian Cancer, Version 2.2020, NCCN Clinical Practice Guidelines in Oncology. *J. Natl. Compr. Cancer Network* **2021**, *19* (2), 191−226.
(23) Herbst, R. S.; Soria, J. C.; Kowanetz, M.; et al. Predictive correlates of response to the anti-PD-L1 antibody MPDL3280A in cancer patients. *Nature* **2014**, *515* (7528), 563−567.
(24) Heinrichs, J.; Bastian, D.; Veerapathran, A.; Anasetti, C.; Betts, B.; Yu, X. Z. Regulatory T-Cell Therapy for Graft-versus-host Disease. *J. Immunol. Res. Ther.* **2016**, *1* (1), 1−14.
(25) Yau, T.; Kang, Y. K.; Kim, T. Y.; et al. Efficacy and Safety of Nivolumab Plus Ipilimumab in Patients With Advanced Hepatocellular Carcinoma Previously Treated With Sorafenib: The CheckMate 040 Randomized Clinical Trial. *JAMA Oncol.* **2020**, *6* (11), No. e204564.
(26) Larkin, J.; Chiarion-Sileni, V.; Gonzalez, R.; Grob, J. J.; Cowey, C. L.; Lao, C. D.; Schadendorf, D.; Dummer, R.; Smylie, M.; Rutkowski, P.; et al. Combined Nivolumab and Ipilimumab or Monotherapy in Untreated Melanoma. *N. Engl. J. Med.* **2015**, *373*, 23−34.
(27) Gandhi, L.; Rodríguez-Abreu, D.; Gadgeel, S.; et al. Pembrolizumab plus Chemotherapy in Metastatic Non-Small-Cell Lung Cancer. *N. Engl. J. Med.* **2018**, *378* (22), 2078−2092.
(28) Paz-Ares, L.; Luft, A.; Vicente, D.; et al. Pembrolizumab plus Chemotherapy for Squamous Non-Small-Cell Lung Cancer. *N. Engl. J. Med.* **2018**, *379* (21), 2040−2051.
(29) West, H.; McCleod, M.; Hussein, M.; et al. Atezolizumab in combination with carboplatin plus nab-paclitaxel chemotherapy compared with chemotherapy alone as first-line treatment for metastatic non-squamous non-small-cell lung cancer (IMpower130): a multicentre, randomised, open-label, phase 3 trial. *Lancet Oncol.* **2019**, *20* (7), 924−937.
(30) Schmid, P.; Adams, S.; Rugo, H. S.; et al. Atezolizumab and Nab-Paclitaxel in Advanced Triple-Negative Breast Cancer. *N. Engl. J. Med.* **2018**, *379* (22), 2108−2121.
(31) Burtness, B.; Harrington, K. J.; Greil, R.; et al. Pembrolizumab alone or with chemotherapy versus cetuximab with chemotherapy for recurrent or metastatic squamous cell carcinoma of the head and neck (KEYNOTE-048): a randomised, open-label, phase 3 study. *Lancet* **2019**, *394* (10212), 1915−1928.
(32) Motzer, R. J.; Tannir, N. M.; McDermott, D. F.; et al. Nivolumab plus Ipilimumab versus Sunitinib in Advanced Renal-Cell Carcinoma. *N. Engl. J. Med.* **2018**, *378* (14), 1277−1290.
(33) Rini, B. I.; Plimack, E. R.; Stus, V.; et al. Pembrolizumab plus Axitinib versus Sunitinib for Advanced Renal-Cell Carcinoma. *N. Engl. J. Med.* **2019**, *380* (12), 1116−1127.
(34) Finn, R. S.; Qin, S.; Ikeda, M.; et al. Atezolizumab plus Bevacizumab in Unresectable Hepatocellular Carcinoma. *N. Engl. J. Med.* **2020**, *382* (20), 1894−1905.
(35) Brahmer, J. R.; Lacchetti, C.; Schneider, B. J.; et al. Management of Immune-Related Adverse Events in Patients Treated With Immune Checkpoint Inhibitor Therapy: American Society of Clinical Oncology Clinical Practice Guideline. *J. Clin. Oncol.* **2018**, *36* (17), 1714−1768.
(36) Hamanishi, J.; Mandai, M.; Iwasaki, M.; et al. Programmed cell death 1 ligand 1 and tumor-infiltrating CD8+ T lymphocytes are prognostic factors of human ovarian cancer. *Proc. Natl. Acad. Sci. U.S.A.* **2007**, *104* (9), 3360−3365.
(37) Wang, Z.; Wu, X. Study and analysis of antitumor resistance mechanism of PD1/PD-L1 immune checkpoint blocker. *Cancer Med.* **2020**, *9* (21), 8086−8121.
(38) Im, S. J.; Hashimoto, M.; Gerner, M. Y.; et al. Defining CD8+ T cells that provide the proliferative burst after PD-1 therapy. *Nature* **2016**, *537* (7620), 417−421.
(39) Riaz, N.; Havel, J. J.; Makarov, V.; et al. Tumor and Microenvironment Evolution during Immunotherapy with Nivolumab. *Cell* **2017**, *171* (4), 934−949.
(40) Shaul, M. E.; Fridlender, Z. G. Tumour-associated neutrophils in patients with cancer. *Nat. Rev. Clin. Oncol.* **2019**, *16* (10), 601−620.
(41) Gungabeesoon, J.; Gort-Freitas, N. A.; Kiss, M.; et al. A neutrophil response linked to tumor control in immunotherapy. *Cell* **2023**, *186* (7), 1448−1464.
(42) Gentles, A. J.; Newman, A. M.; Liu, C. L.; et al. The prognostic landscape of genes and infiltrating immune cells across human cancers. *Nat. Med.* **2015**, *21* (8), 938−945.
(43) Engelmann, C.; Habtesion, A.; Hassan, M.; et al. Combination of G-CSF and a TLR4 inhibitor reduce inflammation and promote regeneration in a mouse model of ACLF. *J. Hepatol.* **2022**, *77* (5), 1325−1338.
(44) Shi, L.; Huang, H.; Lu, X.; Yan, X.; Jiang, X.; Xu, R.; Wang, S.; Zhang, C.; Yuan, X.; Xu, Z.; et al. Effect of human umbilical cord-derived mesenchymal stem cells on lung damage in severe COVID-19 patients: a randomized, double-blind, placebo-controlled phase 2 trial. *Signal Transduct. Targeted Ther.* **2021**, *6* (1), 58.
(45) Wang, T. T.; Zhao, Y. L.; Peng, L. S.; et al. Tumour-activated neutrophils in gastric cancer foster immune suppression and disease progression through GM-CSF-PD-L1 pathway. *Gut* **2017**, *66* (11), 1900−1911.
(46) Shen, D.-D.; Pang, J. R.; Bi, Y. P.; Zhao, L. F.; Li, Y. R.; Zhao, L. J.; Gao, Y.; Wang, B.; Wang, N.; Wei, L.; et al. LSD1 deletion decreases exosomal PD-L1 and restores T-cell response in gastric cancer. *Mol. Cancer* **2022**, *21* (1), 75.
(47) Wang, Y.; Zhou, J.; Tang, C.; et al. Positive effect of Astragaloside IV on neurite outgrowth via talin-dependent integrin signaling and microfilament force. *J. Cell. Physiol.* **2021**, *236* (3), 2156−2168.
(48) Liu, T.; Lu, Y.; Zhan, R.; Qian, W.; Luo, G. Nanomaterials and nanomaterials-based drug delivery to promote cutaneous wound healing. *Adv. Drug Deliv. Rev.* **2023**, *193*, 114670.
(49) Kargl, J.; Zhu, X.; Zhang, H.; Yang, G. H. Y.; Friesen, T. J.; Shipley, M.; Maeda, D. Y.; Zebala, J. A.; McKay-Fleisch, J.; Meredith, G.; et al. Neutrophil content predicts lymphocyte depletion and anti-PD1 treatment failure in NSCLC. *JCI Insight* **2019**, *4* (24), No. e130850.
(50) Blaisdell, A.; Crequer, A.; Columbus, D.; et al. Neutrophils Oppose Uterine Epithelial Carcinogenesis via Debridement of Hypoxic Tumor Cells. *Cancer Cell* **2015**, *28* (6), 785−799.
(51) Zhu, Y.; Huang, J. M.; Zhang, G. N.; Zha, X.; Deng, B. F. Prognostic significance of MyD88 expression by human epithelial ovarian carcinoma cells. *J. Transl. Med.* **2012**, *10*, 77.
(52) Li, C.; Chen, C.; Kang, X.; et al. Decidua-derived granulocyte macrophage colony-stimulating factor induces polymorphonuclear myeloid-derived suppressor cells from circulating CD15+ neutrophils. *Hum. Reprod.* **2020**, *35* (12), 2677−2691.
(53) Wang, Q.; Neubauer, K. J.; Duan, C.; Yin, Q.; Fujitsu, S.; Hosono, H.; Ye, F.; Zhang, R.; Chi, S.; Krycka, K.; et al. Field-induced topological Hall effect and double-fan spin structure with a c-axis component in the metallic kagome antiferromagnetic compound YMn6Sn6. *Phys. Rev. B* **2021**, *103* (1), 014416.

https://doi.org/10.1021/acs.molpharmaceut.5c00681
Mol. Pharmaceutics 2026, 23, 694−710

(54) Bruner, A.; Eger, D.; Oron, M. B.; Blau, P.; Katz, M.; Ruschin, S. Temperature-dependent Sellmeier equation for the refractive index of stoichiometric lithium tantalate. *Opt. Lett.* **2003**, *28* (3), 194−196.
(55) Dai, H.; Yuan, L.; Yin, C.; Cao, Z.; Chen, X. Direct Visualizing the Spin Hall Effect of Light via Ultrahigh-Order Modes. *Phys. Rev. Lett.* **2020**, *124* (5), 053902.

https://doi.org/10.1021/acs.molpharmaceut.5c00681
Mol. Pharmaceutics 2026, 23, 694−710